TiS Trends in Sciences
TRENDS IN SCIENCES 2027; 24(1): 14004
SPRINT Scholarly Publishing and Repository Integration Center
https://doi.org/10.48048/tis.2027.14004
RESEARCH ARTICLE

A Comparative Evaluation of the Vasorelaxant Effects of F-1 and F-3 on Aorta and Pulmonary artery: Integrated *In Vitro*, *In Vivo* and *In Silico* Approaches

Bakiyeva Muazzam Sharifjanovna[1*], Gusakova Svetlana Valeryevna[2], Sherzod Niyatqobulovich Zhurakulov[3], Rustamova Shohista Omonjonovna[1], Mavlanova Sadbarxon Abdukarimovna[1], Sharipova Nazifa Nasimovna[1], Xodjayeva Naimaxon Umirzaqovna[1], Xafizova Klaraxon Abdumannabovna[1], Xayitbayev Azamat Madaminovich[1,4], Dadamirzayeva Kamola Abduhalimovna[1], Yunusova Rayhona Melsbek qizi[1] and Xolmirzyeva Nazira Azimjon qizi[1]

[1]*Faculty of Medicine, Namangan State University, Namangan, Uzbekisan*
[2]*Faculty of Medicine, Siberian State University, Russia*
[3]*Institute of the Chemistry of Plant Substances, Academy of Sciences of the Republic of Uzbekistan, Tashkent, Uzbekistan*
[4]*Faculty of Medicine, Impuls Medical University, Namangan, Uzbekistan*

([*]Corresponding author's e-mail: bakiyevamsh@mail.ru)

Received: 6 April 2026, Revised: 22 May 2026, Accepted: 1 June 2026, Published: 25 August 2026

Abstract

This study aimed to evaluate the vasomodulatory and antihypertensive effects of compounds 1-Phenyl-6,7-dimethoxy-1,2,3,4-tetrahydroisoquinoline hydrochloride (F-1) and 1-(3′-hydroxyphenyl)-6,7-dimethoxy-1,2,3,4-tetrahydroisoquinoline hydrochloride (F-3) using an integrated approach combining *in silico* molecular docking, *in vitro* functional assays, and *in vivo* experimental models. Molecular docking analysis revealed that both compounds exhibit high binding affinity toward calcium-regulating targets, particularly the L-type calcium channel (Cav1.2), with binding energies of −8.2 kcal/mol (F1) and −8.1 kcal/mol (F3), indicating stable ligand–protein interactions and potential modulation of calcium influx. *In vitro* experiments demonstrated that both compounds significantly inhibited phenylephrine-induced vascular smooth muscle contraction in a concentration-dependent manner. F1 exhibited higher potency (IC_{50} = 3.1×10^{-7} M) compared to F3 (IC_{50} = 4.29×10^{-6} M), showing a more consistent and gradual inhibitory profile. Additionally, both compounds enhanced the vasorelaxant effect of verapamil and partially attenuated the inhibitory action of phentolamine, suggesting involvement in both calcium channel modulation and adrenergic signaling pathways. The reduction of their effects in the presence of L-NAME indicates partial dependence on nitric oxide-mediated mechanisms. *In vivo* studies in adrenaline-induced hypertensive rats demonstrated that F1 and F3 significantly reduced systolic and diastolic blood pressure in a dose- and time-dependent manner at doses of 10, 25, and 50 mg/kg. F1 showed a more pronounced antihypertensive effect, effectively restoring blood pressure toward physiological levels. Overall, the findings indicate that F1 is a more potent vasorelaxant and antihypertensive agent than F3. The observed effects are mediated through a multi-target mechanism involving inhibition of calcium influx, modulation of adrenergic signaling, and partial involvement of nitric oxide pathways. These results highlight F1 as a promising candidate for the development of novel therapeutic agents for the treatment of hypertension and vascular dysfunction.

Keywords: F-1 compound, F-3 compound, Vasorelaxation, Vascular smooth muscle, Aorta, Pulmonary artery, Molecular docking

Introduction

A regulation of vascular tone is a key factor in maintaining cardiovascular homeostasis and is primarily controlled by the contractile state of vascular smooth muscle cells. One of the main mechanisms underlying smooth muscle contraction is the influx of calcium ions through voltage-dependent calcium channels, particularly L-type calcium channels. These channels play a central role in both systemic and pulmonary circulation, including the aorta and pulmonary artery, by regulating vasoconstriction and vasodilation processes [1]. Dysfunction of calcium handling in vascular smooth muscle is closely associated with various cardiovascular disorders, such as hypertension and pulmonary arterial hypertension. Therefore, modulation of calcium channels remains an important pharmacological target for the development of new therapeutic agents. In recent years, increasing attention has been given to biologically active compounds capable of influencing vascular tone through different molecular mechanisms, including calcium channel inhibition. Among such compounds, derivatives containing phenolic and isoquinoline structures have demonstrated promising pharmacological activities, including vasorelaxant and antioxidant effects. In this context, the present study focuses on 2 biologically active compounds, F-1 and F-3, whose potential effects on vascular smooth muscle have not been fully characterized [2]. To obtain a comprehensive understanding of their pharmacological properties, an integrated experimental approach was applied. The effects of F-1 and F-3 were investigated using isolated aortic and pulmonary artery preparations (*in vitro*), supported by *in vivo* studies to evaluate systemic vascular responses [3]. Furthermore, molecular docking analysis was performed to explore the interaction of these compounds with L-type calcium channels at the molecular level. The aim of this study was to evaluate the effects of F-1 and F-3 on vascular smooth muscle and to elucidate their possible mechanisms of action through combined *in vitro*, *in vivo*, and *in silico* approaches.

Materials and methods

Chemicals

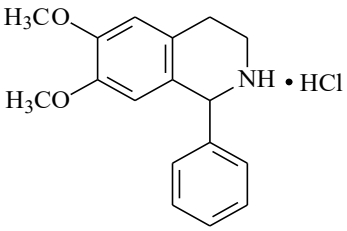
F-1 and F-3 were used as test compounds in the present study. The purity of both compounds was 95%. Stock and working solutions of F-1 and F-3 were prepared by dissolving the compounds in distilled water. The required concentrations were freshly prepared before each experiment. Other chemicals and reagents used in the experiments were of analytical grade.

Acute toxicity and behavioral effects of 1-Phenyl-6,7-dimethoxy-1,2,3,4-tetrahydroisoquinoline hydrochloride (F-1)

Acute Toxicity and Behavioral Effects of 1-Phenyl-6,7-dimethoxy-1,2,3,4-tetrahydroisoquinoline hydrochloride (F-1) The acute toxicity of the selected compound (F1) was studied in outbred white male mice weighing 18 - 20 g. The compound was administered at doses of 100.0, 200.0, 225.0, 250.0, 280.0, 300.0, 325.0, and 350.0 mg/kg. When the compound was administered at a dose of 100.0 mg/kg, noticeable changes were observed in the general condition and behavior of intact animals, including drowsiness, mild tremor, marked depression of general condition, reduced locomotor activity, increased muscle tone, and short-term acceleration of respiration. With increasing doses (starting from 200.0 mg/kg), further deterioration in the general condition of animals was observed, characterized by pronounced drowsiness, decreased motor activity, tremor, and convulsions. At a dose of 225.0 mg/kg, which was identified as the initial lethal dose, animals exhibited decreased responsiveness to external stimuli and pain, along with reduced general condition, drowsiness, decreased locomotor activity, tremor, and convulsions. Mortality was observed in 1 out of 6 animals. At a dose of 250.0 mg/kg, mortality increased to 2 out of 6 animals. Experimental results demonstrated that the median lethal dose (LD_{50}) of the studied compound in mice was approximately 280.0 mg/kg. At a dose of 300.0 mg/kg, animals showed severe deterioration in general condition, persistent drowsiness, reduced locomotor activity, and prolonged tremor and convulsions, with mortality observed in 4 out of 6 animals. At 325.0 mg/kg, similar symptoms were observed, including prolonged convulsions and lateral positioning of the animals; mortality reached 5 out of 6 mice. At higher doses, prolonged convulsions were

noted, and the onset of mortality began from approximately the 60th minute after administration. Administration of the compound at a dose of 350.0 mg/kg resulted in 100% mortality of the experimental animals (**Table 1**).

Table 1 Acute toxicity study of 1-phenyl-6,7-dimethoxy-1,2,3,4-tetrahydroisoquinoline hydrochloride (F-1).

Name of ligand	Chemical structure	Dose mg/kg	Animal mortality/survival	LD_{50}
1-Phenyl-6,7-dimethoxy-1,2,3,4-tetrahydroisoquinoline hydrochloride (F-1)		100.0	0/6	273.2 (249.7 ± 296.7)
		200.0	0/6	
		225.0	1/5	
		250.0	2/4	
		280.0	3/3	
		300.0	4/2	
		325.0	5/1	
		350.0	6/0	

The statistical analysis of the obtained data was performed using IBM® SPSS® Statistics software, version 27.0.1.0.

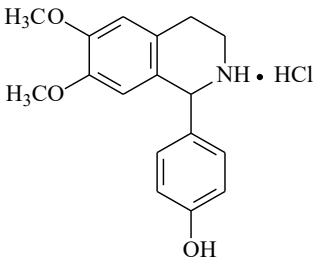
Acute toxicity of 1-(3'-hydroxyphenyl)-6,7-dimethoxy-1,2,3,4-tetrahydroisoquinoline hydrochloride (F-3)

The experiments were conducted on outbred white male mice weighing 18 - 20 g. The compound was administered at doses of 100.0, 200.0, 300.0, 400.0, 500.0, 600.0, 700.0, 800.0, 850.0, 900.0, 925.0, 950.0, 975.0, 1,000.0, and 1,050.0 mg/kg. Six mice were used for each dose of the compound.

Toxicity profile

The results of the experiments showed that administration of 1-(3'-hydroxyphenyl)-6,7-dimethoxy-1,2,3,4-tetrahydroisoquinoline hydrochloride (F-3) at a dose of 100 mg/kg caused an increase in respiration rate and a significant decrease in locomotor activity within 5 - 7 min. The response to external stimuli remained within physiological limits. No mortality was observed in experimental animals over a 14-day observation period. Increasing the dose to 200.0, 300.0, 400.0, 500.0, and 600.0 mg/kg led to the appearance of tremor in the head region within 10 - 15 min after administration, and in some animals, clonic convulsions were observed. At doses of 700.0 - 800.0 - 850.0 mg/kg, further effects included reduced locomotor activity, tremor, increased muscle tone in the tail and certain muscle groups, and clonic convulsions. To determine acute toxicity, increasing the oral dose of the compound to 875.0 mg/kg resulted in clonic convulsions within 17 - 24 h. At this dose, mortality was observed in 1 out of 6 animals. The condition of the surviving animals returned to normal by the second day. Further dose escalation led to an increase in the toxic effects of the compound. At an oral dose of 900.0 mg/kg, mortality was observed in 2 out of 6 animals. At 925.0 mg/kg, 3 out of 6 animals died by the second day of observation. At 950.0 mg/kg, mortality increased to 4 out of 6 animals. At 975.0 mg/kg, 5 out of 6 animals died. A 100% mortality rate was observed at a dose of 1,050.0 mg/kg.

Table 2 Acute toxicity study of 1-(3'-hydroxyphenyl)-6,7-dimethoxy-1,2,3,4-tetrahydroisoquinoline hydrochloride (F-3).

Name of ligand	Chemical structure	Dose mg/kg	Animal mortality/survival	LD_{50}
1-(3′-hydroxyphenyl)-6,7-dimethoxy-1,2,3,4-tetrahydroisoquinoline hydrochloride **(F-3)**		100.0	0/6	924.2 (893.9 ± 953.9)
		200.0	0/6	
		300.0	0/6	
		400.0	0/6	
		500.0	0/6	
		600.0	0/6	
		700.0	0/6	
		800.0	0/6	
		875.0	1/5	
		900.0	2/4	
		925.0	3/3	
		950.0	4/2	
		975.0	5/1	
		1050.0	6/0	

The acute toxicity results showed a marked difference between F-1 and F-3. The LD50 value of F-1 was 273.2 mg/kg, whereas that of F-3 was 924.2 mg/kg, indicating that F-3 had a considerably lower acute toxicity profile than F-1. This difference may be related to structural variation between the 2 compounds, particularly the presence of the hydroxyphenyl group in F-3, which may influence solubility, distribution, metabolism, and overall toxicological response. The higher LD50 value of F-3 suggests a wider safety margin compared with F-1. However, further toxicokinetic and mechanistic toxicity studies are required to fully explain the basis of this difference.

Animal ethics

All experimental procedures were approved by the Animal Ethics Committee of the Institute of Bioorganic Chemistry, Academy of Sciences of the Republic of Uzbekistan (Protocol No. 133/1a/h, dated August 4, 2014). All surgical manipulations were performed under sodium pentobarbital anesthesia, and appropriate measures were taken to reduce animal suffering. Male white rats weighing 200 - 250 g were used in the experiments.

Tissue preparation

All surgical procedures were performed under sodium pentobarbital anesthesia to ensure the absence of pain and minimize animal suffering. The study utilized thoracic aortic tissue obtained from healthy adult male Wistar rats weighing 200 - 250 g. Euthanasia was carried out by cervical dislocation. Following thoracotomy, the aorta was carefully excised, thoroughly cleared of surrounding perivascular adipose and connective tissues, and cut into vascular rings of approximately 3 - 4 mm in length [4]. These aortic rings were then placed in a 5 mL organ bath containing Krebs–Henseleit physiological solution composed of (in mM): NaCl 120.4, KCl 5, $NaHCO_3$ 15.5, NaH_2PO_4 1.2, $MgCl_2$ 1.2, $CaCl_2$ 2.5, glucose 11.5, and HEPES, adjusted to pH 7.4 [5,6]. In selected experiments, a calcium-free Krebs solution supplemented with 1 mM EGTA was used to evaluate calcium-dependent responses. During the experiments, the organ bath solution was continuously aerated with carbogen gas (5% CO_2 and 95% O_2) and maintained at a constant temperature of 37 °C using a DAIHAN ultrathermostatic water bath system [7].

Aortic-ring and Pulmonary artery contraction studies

Aortic and pulmonary artery rings were mounted in a Radnoti isometric transducer system (USA) using platinum wire hooks and allowed to equilibrate for 60 minutes under standard physiological conditions [8]. Each tissue sample was initially stretched to a resting

tension of 1 g (10 mN). The contractile responses were recorded via the isometric transducer, transmitted to a signal amplifier, and digitized using a Go-link analog-to-digital converter connected to a computer. Data acquisition and analysis were performed using OriginPro software, version 8.5 SR1 (EULA, Northampton, MA, USA) [9]. The contractile tension of both aortic and pulmonary artery tissues *in vitro* was expressed as a percentage for statistical evaluation. The functionality of vascular smooth muscle was verified using an experimental setup based on the method described by. The 5 mL organ bath was integrated into a recirculating system containing Krebs–Henseleit solution. The temperature was strictly maintained using a thermostat, while the solution was continuously aerated with a gas mixture of 95% O_2 and 5% CO_2 [10]. Isometric tension of the mounted aortic and pulmonary artery segments was continuously recorded using a Grass Instruments isometric transducer (USA) and monitored through the GoLink data acquisition and amplification system [11].

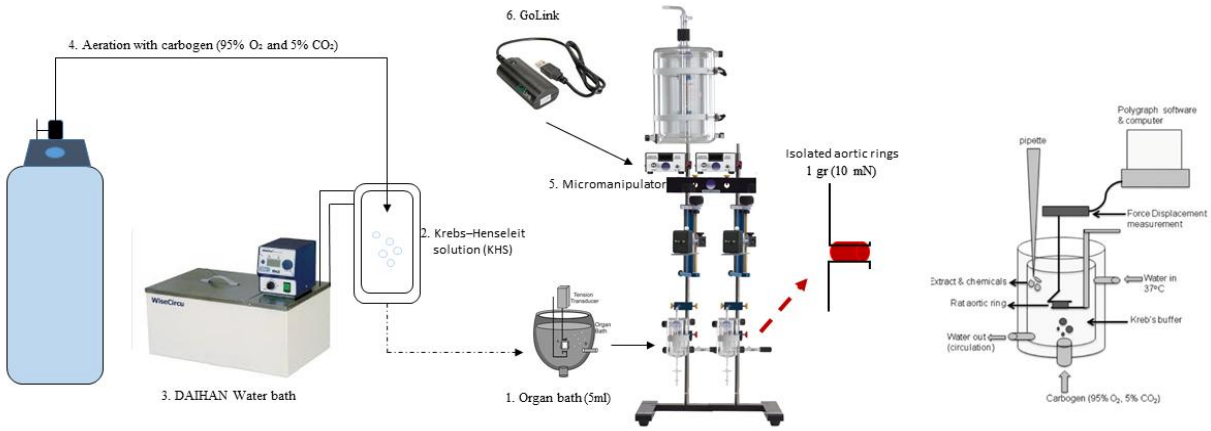


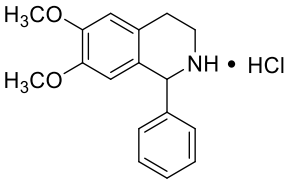
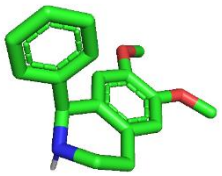
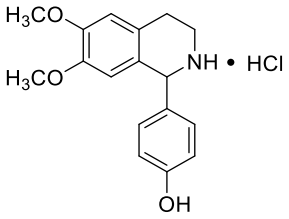
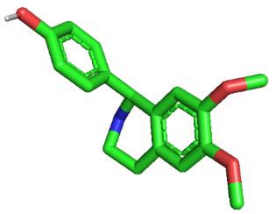
Figure 1 A schematic illustration of the apparatus used to regulate and measure the isometric contraction of isolated rat aortic vascular muscle. 1) The organ bath (5 mL) circulates through a specialized reservoir. 2) The Krebs-Henseleit solution ensures physiological conditions. 3) A thermostat maintains a constant physiological temperature. 4) The system is aerated with a gas mixture of 5% CO_2 and 95% O_2. The contractile activity of the aortic preparation is secured in the experimental chamber. 5) An isometric transducer (Grass Instrument, USA) monitors the contraction, and 6) GoLink devices provide signal amplification.

Molecular docking "software and databases"

All computational tools used in this study were freely available for academic research purposes. The 3-dimensional structures of the target proteins were obtained from the Protein Data Bank (PDB), an internationally recognized repository of structural data for biological macromolecules. Considering the central role of calcium ions in the regulation of vascular smooth muscle contraction and relaxation, 2 calcium channel proteins were selected for *in silico* analysis: The L-type voltage-gated calcium channel (Cav1.2, PDB ID: 6jp5) and the R-type calcium channel (Cav2.3, PDB ID: 7xlq) [12]. The chemical structures of the investigated compounds, including the studied flavonoids and reference molecules, were retrieved from the PubChem database. PubChem provides a comprehensive platform integrating chemical, pharmacological, and bioinformatic data, including physicochemical properties and biological activity profiles of small molecules and their interactions with target proteins [13]. All protein structures downloaded in PDB format were carefully examined and prepared using PyMOL (version 1.2), a Python-based molecular visualization software (www.pymol.org). PyMOL was also utilized for visualization and analysis of ligand–protein docking interactions. Molecular docking studies were carried out using AutoDock 4.2, developed by The Scripps Research Institute (www.scripps.edu). AutoDock Tools (ADT) was employed as a graphical interface to prepare protein and ligand structures, assign partial charges, define rotatable bonds, and conFigure grid box parameters [14]. This software enables the prediction of

the most favorable binding conformations and interactions between small molecules and target proteins with known 3-dimensional structures [15].

Table 3 3D and 2D structure of 1-Phenyl-6,7-dimethoxy-1,2,3,4-tetrahydroisoquinoline hydrochloride (F-1) and 1-(3′-hydroxyphenyl)-6,7-dimethoxy-1,2,3,4-tetrahydroisoquinoline hydrochloride (F-3).

Ligands	2D	3D
1-Phenyl-6,7-dimethoxy-1,2,3,4-tetrahydroisoquinoline hydrochloride (F-1)		
1-(3′-hydroxyphenyl)-6,7-dimethoxy-1,2,3,4-tetrahydroisoquinoline hydrochloride (F-3)		

Preparation of ligand and protein files

Before docking could be performed, the retrieved PDB structures required preprocessing, as files obtained from the Protein Data Bank are typically not directly suitable for docking studies. Structural issues such as missing hydrogen atoms, the presence of crystallographic water molecules, co-crystallized ligands, ions, and additional non-relevant heteroatoms necessitated correction. Each protein structure was imported into AutoDock Tools (ADT). Crystallographic water molecules and non-essential heteroatoms were removed. Co-crystallized ligands were deleted prior to docking calculations; however, they were retained separately for validation purposes when applicable. All crystallographic heteroatoms, including calcium ions and other non-protein components, were removed during receptor preparation to avoid potential artificial electrostatic bias in docking simulations under the rigid receptor model. This approach ensured consistent electrostatic treatment across all targets. The structures were visually inspected in PyMOL to evaluate missing residues, and no critical residues within the functional or channel pore regions were absent in the selected models. Polar hydrogen atoms were added, and Kollman united atom charges were assigned to the protein structures to ensure appropriate electrostatic representation. Protonation states were adjusted to approximate physiological pH (7.4) conditions according to the standard procedures implemented in AutoDock Tools. The prepared receptor file was then saved in the .pdbqt format, which includes atom types and partial charge information required for docking calculations. Ligand structures underwent a comparable preparation process. The molecules were loaded into ADT, hydrogens were added, and Gasteiger charges were assigned. Nonpolar hydrogens were merged according to standard AutoDock protocols. ADT automatically identified the appropriate rotatable bonds and root atom for each ligand. The final ligand files were exported in the .pdbqt format, containing structural coordinates, rotatable bond definitions, and assigned partial charges necessary for docking simulations [12].

Calculation of inhibition constant (Ki) from binding energy

In molecular docking analyses, the interaction strength between a ligand and its target protein is commonly represented as the binding free energy (ΔG), expressed in kcal/mol. The corresponding inhibition constant (Ki) can be theoretically estimated from the calculated binding energy by applying the standard thermodynamic equation. Ki represents a computational indicator of ligand–target binding affinity under equilibrium assumptions. A lower Ki value generally suggests stronger predicted interaction and higher binding affinity. However, in docking studies, Ki should

be interpreted only as a theoretical parameter derived from binding energy. Therefore, Ki values are useful for comparing the relative binding tendencies of different ligands toward the same target, but they require experimental validation through biochemical, biophysical, or functional assays.

$$Ki = e^{\frac{\Delta G \times 1{,}000}{R \times T}}$$

where Ki is the inhibition constant (in mol/L); ΔG is the binding free energy (in kcal/mol); R is the universal gas constant = 1.987 cal/(mol·K); T is the temperature in Kelvin (usually 298.15 K); The factor 1,000 converts kcal to cal.

Statistics

Statistical analysis and graphical representations were performed using OriginPro version 9 (USA). Vascular contractile responses were expressed as a percentage of the maximal contraction induced by phenylephrine (10 mM) or potassium chloride (50 mM). All results are presented as the mean of 4 - 6 independent experiments (n = 4 - 6). Statistical comparisons within groups were carried out using paired t-tests, whereas differences between independent experimental groups were analyzed using unpaired t-tests. A *p*-value of less than 0.05 was considered statistically significant [17].

Results and discussion

Effect of F-1 and F-3 on aortic smooth muscle

The effects of the tested compounds on aortic contraction were investigated under conditions of potassium chloride (30 μM)-induced tone. The data revealed distinct dose–response profiles for F1 and F3, indicating differences in their pharmacological potency and efficacy [18]. F1 exhibited a clear and progressive concentration-dependent inhibitory effect on aortic contraction. At the lowest concentration tested (1×10^{-9} M), the contraction force was 96.56%, followed by a slight decrease to 90.4% and 89.2% at 1×10^{-8} and 1×10^{-7} M, respectively. As the concentration increased, a marked reduction in contraction was observed, with values declining to 65.7% at 1×10^{-6} M and 42.7% at 1×10^{-5} M. This inhibitory trend continued at higher concentrations, reaching 23% at 1×10^{-4} M and nearly complete suppression (0.86%) at 0.001 M. The calculated IC50 value of 4.7×10^{-6} M indicates a high potency of F1 in reducing vascular contraction. In contrast, F3 demonstrated a markedly different response pattern. The contraction force remained largely unchanged across lower and intermediate concentrations, with values of 98.36%, 99.3%, and 98.4% at 1×10^{-9}, 1×10^{-8}, and 1×10^{-7} M, respectively. Even at higher concentrations, only a modest decrease was observed, with contraction forces of 96.5% at 1×10^{-6} M, 94.7% at 1×10^{-5} M, and 92.16% at 1×10^{-4} M. A pronounced inhibitory effect appeared only at the highest concentration (0.001 M), where contraction dropped sharply to 18%. The IC50 value for F3 was determined to be 3.7×10^{-4} M, reflecting a substantially lower potency compared to F1 (**Figure 2(a)**). Taken together, these findings indicate that F1 exerts a strong and gradual inhibitory effect on potassium chloride-induced aortic contraction, whereas F3 remains largely ineffective at lower concentrations and only demonstrates significant activity at higher doses. This suggests that F1 has a greater pharmacological efficacy and potency in modulating vascular smooth muscle contraction under the given experimental conditions.

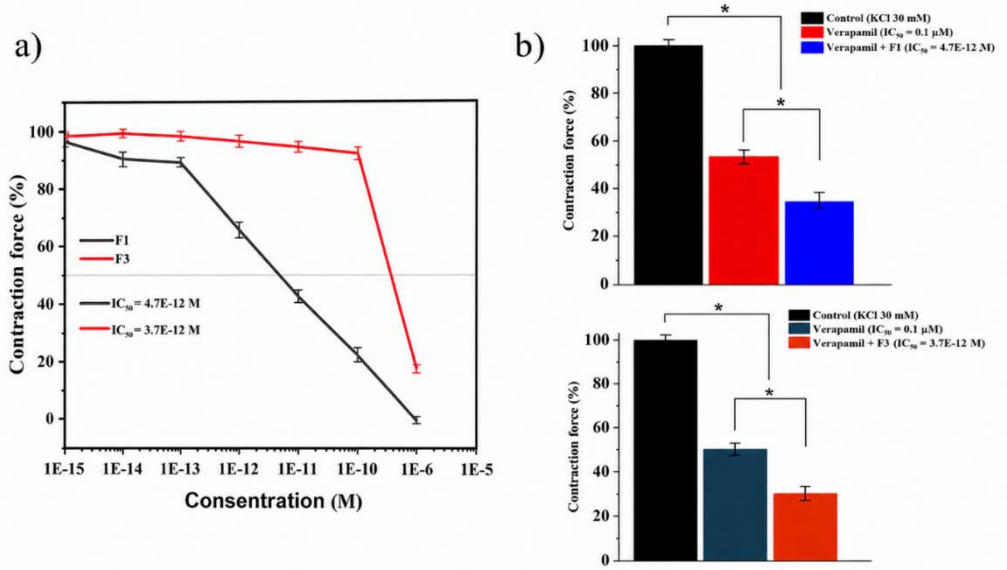


Figure 2 (a) F1 and F3 suppress KCl-evoked vascular contraction, (b) enhance verapamil-mediated Ca^{2+} channel blockade ($p < 0.05$).

The relaxant effects of verapamil alone and in combination with F1 and F3 on contraction force were evaluated. The maximal contraction induced by 30 mM KCl was taken as the baseline and defined as the control group (100 ± 2.4%). Administration of verapamil at its half-maximal inhibitory concentration (IC_{50} = 0.1 µM) significantly reduced the contraction force to 53.3 ± 2.9% compared to the KCl-induced control. Co-application of verapamil with F1 (IC_{50} = 4.7×10^{-6} M) resulted in a further decrease in contraction force to 35.1 ± 3.1%. Similarly, the combination of verapamil with F3 (IC_{50} = 3.7×10^{-4} M) produced an even more pronounced inhibitory effect, reducing the contraction force to 30.1 ± 3.1%. Statistical analysis demonstrated that both combination treatments significantly attenuated contraction compared to the control group. Importantly, the reductions observed in the verapamil + F1 and verapamil + F3 groups were also statistically significant when compared with verapamil alone. Notably, the combination with F3 exhibited a stronger inhibitory effect than F1, indicating a comparatively higher potentiating capacity (**Figure 2(b)**). These findings clearly suggest that both F1 and F3 enhance the vasorelaxant effect of verapamil, likely through synergistic inhibition of voltage-dependent Ca^{2+} channels, leading to reduced Ca^{2+} influx into vascular smooth muscle cells.

The effects of the tested compounds on aortic contraction were assessed under phenylephrine (1 µM)-induced tone [19]. The results demonstrated clear differences in both potency and the pattern of response between F1 and F3 across the tested concentration range. F1 produced a consistent and concentration-dependent reduction in contraction force. At 1×10^{-9} M, the contraction level was 73.8%, which gradually decreased to 65.9% and 55.9% at 1×10^{-8} and 1×10^{-7} M, respectively. With further increases in concentration, a more pronounced inhibitory effect was observed, reaching 44.1% at 1×10^{-6} M and 21.5% at 1×10^{-5} M. At higher concentrations, the contraction force declined further to 13.7% at 1×10^{-4} M and nearly complete inhibition (0.87%) at 0.001 M. The calculated IC50 value for F1 was 3.1×10^{-7} M, indicating high potency under these experimental conditions. In contrast, F3 maintained a high level of contraction at lower concentrations, with values of 99.4%, 98.54%, and 95.6% at 1×10^{-9}, 1×10^{-8}, and 1×10^{-7} M, respectively. A noticeable decrease began at 1×10^{-6} M, where contraction dropped to 57.4%, followed by further reductions to 45.2% at 1×10^{-5} M and 40.4% at 1×10^{-4} M. At the highest concentration (0.001 M), contraction was almost completely suppressed, reaching 0.21%. The IC50 value for F3 was 4.29×10^{-6} M, reflecting a lower potency compared to F1 (**Figure 2(a)**). Overall, both compounds exhibited inhibitory effects on phenylephrine-induced aortic contraction; however, F1 showed a stronger and more gradual dose-dependent response, while F3 displayed minimal effects at lower

concentrations followed by a sharper decline at higher doses. These findings suggest that F1 is more potent and effective in reducing vascular smooth muscle contraction in this experimental model.

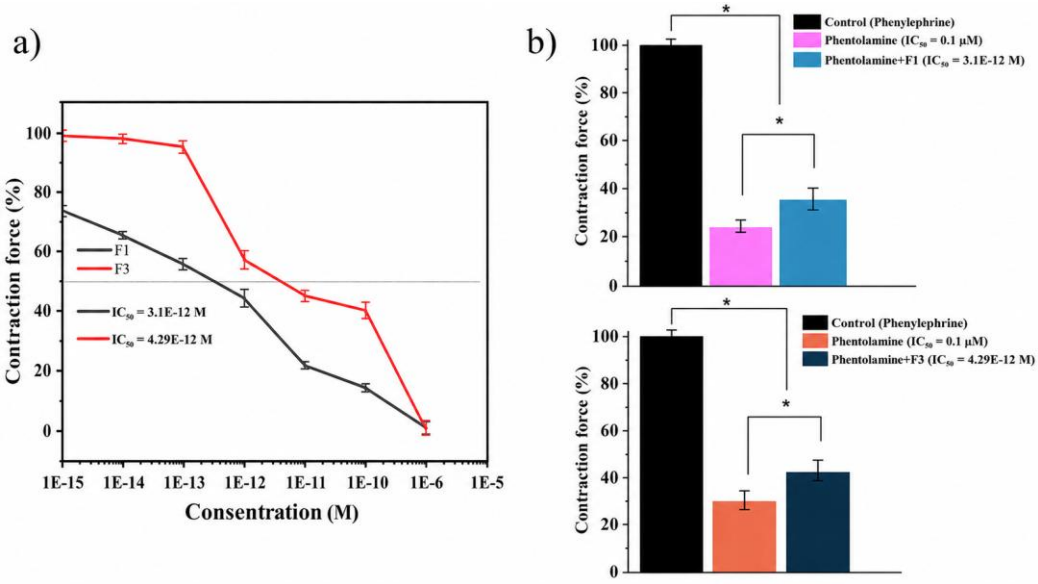


Figure 3 (a) concentration-dependent inhibition of phenylephrine-induced contraction by F1 and F3, (b) their interaction with phentolamine in isolated rat aortic rings ($p < 0.05$).

The modulatory effects of phentolamine alone and in combination with F1 and F3 on contraction force were evaluated using phenylephrine-induced contraction as the reference. The maximal contraction induced by phenylephrine was taken as the baseline and defined as the control group (100 ± 1.8%). Administration of the non-selective α-adrenergic antagonist phentolamine at its half-maximal inhibitory concentration (IC_{50} = 0.1 μM) markedly reduced the contraction force to 25.3 ± 2.1% compared to the control. Co-application of phentolamine with F1 ($IC_{50} = 3.1\times10^{-7}$ M) resulted in an increased contraction force of 35.7 ± 3.6%. Similarly, the combination of phentolamine with F3 ($IC_{50} = 4.29\times10^{-6}$ M) led to a further increase in contraction force to 40.7 ± 3.2%. Statistical analysis demonstrated that, although both combination groups remained significantly lower than the control, the contraction force in the phentolamine + F1 and phentolamine + F3 groups was significantly higher than that observed with phentolamine alone (**Figure 3(b)**). Notably, the effect was more pronounced in the presence of F3 compared to F1. These findings indicate that both F1 and F3 partially attenuate the inhibitory effect of phentolamine on phenylephrine-induced contraction. This suggests that the tested compounds may modulate α-adrenergic signaling or influence downstream pathways involved in vascular smooth muscle contraction, partially counteracting the blockade induced by phentolamine.

Study the role of endothelium in the relaxant effect of F1 and F3

The dose–response effects of the tested compounds on aortic contraction were evaluated in the presence of the nitric oxide synthase inhibitor L-NAME (1 μM) under potassium chloride (30 μM)-induced tone [20]. These conditions allowed assessment of the role of nitric oxide in modulating vascular responses to F1 and F3. F1 demonstrated a clear concentration-dependent inhibitory effect on aortic contraction, although the overall potency appeared reduced compared to conditions without L-NAME. At 1×10^{-9} M, the contraction force was 99.8%, followed by a gradual decrease to 94.7% and 88.2% at 1×10^{-8} and 1×10^{-7} M, respectively. With increasing concentration, a more pronounced decline was observed, reaching 60.5% at 1×10^{-6} M and 57% at 1×10^{-5} M. At higher concentrations, the contraction force further decreased to 36.4% at 1×10^{-4} M and complete inhibition (0%) at 0.001 M. The calculated IC50 value for F1 was 2.26×10^{-5} M, indicating a shift toward lower potency in the presence of L-NAME. F3 exhibited a different response profile, maintaining relatively high contraction

levels across low and intermediate concentrations. The contraction force was 97.9% at 1×10^{-9} M, 90.7% at 1×10^{-8} M, and remained around 90% at 1×10^{-7} and 1×10^{-6} M. A moderate decrease was observed at 1×10^{-5} M (87.4%), followed by a more substantial reduction to 63.2% at 1×10^{-4} M. At the highest concentration (0.001 M), contraction decreased to 23.3%. The IC50 value for F3 was 2.17×10^{-4} M, confirming lower potency compared to F1 (**Figure 4(a)**). Overall, both compounds retained their ability to inhibit potassium chloride-induced aortic contraction in the presence of L-NAME; however, their potencies were reduced, particularly for F1. This shift suggests that nitric oxide plays a significant role in mediating the vasorelaxant effects of these compounds. The attenuation of activity after nitric oxide synthase inhibition indicates that part of the mechanism of action of F1 and, to a lesser extent, F3, may involve endothelium-dependent pathways associated with nitric oxide production.

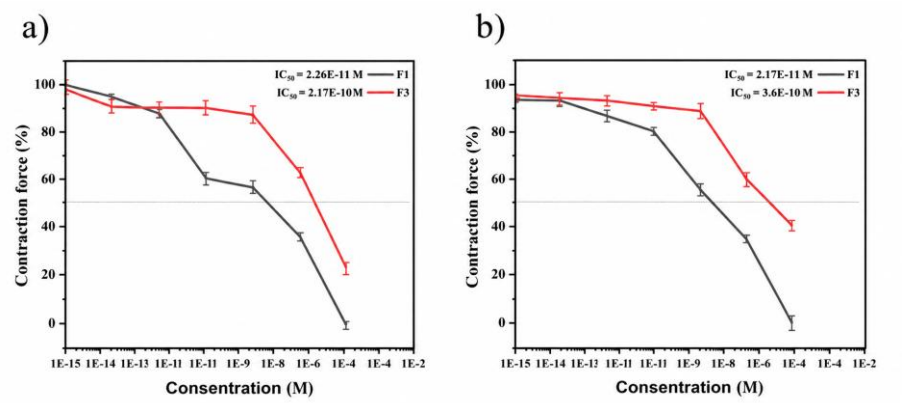


Figure 4 Effect of F1 and F3 on potassium chloride-induced aortic contraction in the presence of L-NAME (1 μM), Effect of F1 and F3 on phenylephrine (1 μM)-induced contraction in aortavein tissue in the presence of L-NAME (1 μM).

The effects of F1 and F3 on aortic contraction were studied under phenylephrine (1 μM)-induced conditions in the presence of the nitric oxide synthase inhibitor L-NAME (1 μM) [21]. This experimental setup was used to evaluate the involvement of nitric oxide in the vasorelaxant responses of the compounds. F1 produced a concentration-dependent decrease in contraction, although its potency was reduced compared to conditions without L-NAME. At lower concentrations (1×10^{-9} - 1×10^{-8} M), the contraction remained relatively stable at around 94% - 95%, followed by a gradual decline to 88.2% at 1×10^{-7} M and 81.9% at 1×10^{-6} M. A stronger inhibitory effect became evident at higher concentrations, with contraction decreasing to 57% at 1×10^{-5} M and 36.4% at 1×10^{-4} M, eventually reaching complete inhibition at 0.001 M. The IC50 value of 2.17×10^{-5} M reflects a reduction in potency in the presence of L-NAME. In comparison, F3 showed a less pronounced effect at lower concentrations, maintaining contraction levels above 90% from 1×10^{-9} to 1×10^{-5} M. A noticeable decrease occurred only at higher concentrations, with contraction dropping to 60.9% at 1×10^{-4} M and further to 40.9% at 0.001 M. The IC50 value for F3 was 3.6×10^{-4} M, indicating lower potency relative to F1 (**Figure 4(b)**). In general, both compounds were able to reduce phenylephrine-induced contraction even in the presence of L-NAME, but their effectiveness was diminished. This reduction suggests that nitric oxide plays an important role in their mechanism of action, and that the vasorelaxant effects of F1 and F3 are at least partly dependent on nitric oxide-mediated pathways.

Effect of F-1 and F-3 on Pulmonary artery

The effects of F1 and F3 on Pulmonary artery contraction were evaluated under potassium chloride (15 μM)-induced conditions, revealing clear differences in their concentration–response profiles [21]. F1 demonstrated a pronounced concentration-dependent decrease in contraction force. The contraction level was 90.9% at 1×10^{-9} M, which decreased to 82.6% at 1×10^{-8} M and 77% at 1×10^{-7} M. With further increases in concentration, a stronger inhibitory effect was observed, reaching 62.7% at 1×10^{-6} M and 40.5% at 1×10^{-5} M. At

higher concentrations, contraction declined further to 30% at 1×10^{-4} M and was completely abolished (0%) at 0.001 M. In contrast, F3 showed relatively minor changes at lower concentrations, with contraction values of 96.3% at 1×10^{-9} M, 94.7% at 1×10^{-8} M, and 92.1% at 1×10^{-7} M. The contraction remained largely stable at 1×10^{-6} M (92.4%) and slightly decreased to 87.1% at 1×10^{-5} M. A more noticeable reduction was observed at higher concentrations, with contraction decreasing to 84.3% at 1×10^{-4} M and 25.3% at 0.001 M (**Figure 5(A)**). Overall, both F1 and F3 reduced potassium chloride-induced contraction in Pulmonary artery tissue; however, F1 exhibited a stronger and more progressive dose-dependent inhibitory effect. In contrast, F3 showed limited activity at lower concentrations and a more marked effect only at higher doses.

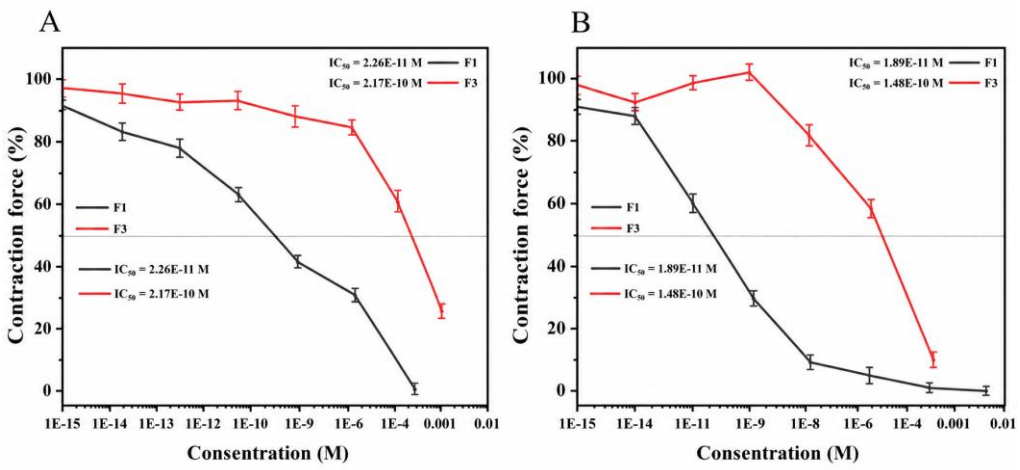


Figure 5 Effect of F1 and F3 on potassium chloride (15 μM)-induced contraction in Pulmonary artery tissue (A), effect of F1 and F3 on phenylephrine (1 μM)-induced contraction in Pulmonary artery tissue (B).

The effects of F1 and F3 on Pulmonary artery contraction were evaluated under phenylephrine (1 μM)-induced conditions, demonstrating clear differences in their concentration–response relationships. F1 showed a strong concentration-dependent decrease in contraction force. The contraction level was 90.3% at 1×10^{-9} M and slightly decreased to 87.6% at 1×10^{-8} M. A more pronounced reduction was observed at 1×10^{-7} M (59.1%), followed by a sharp decline to 27.7% at 1×10^{-6} M. At higher concentrations, the contraction dropped further to 6.6% at 1×10^{-5} M and 4.2% at 1×10^{-4} M, reaching 1.7% at 0.001 M, indicating near-complete inhibition. In contrast, F3 maintained high contraction levels at lower concentrations, with values of 96% at 1×10^{-9} M, 90.9% at 1×10^{-8} M, and 96.7% at 1×10^{-7} M. The contraction remained elevated at 1×10^{-6} M (99.1%), followed by a noticeable decrease at higher concentrations, reaching 78.3% at 1×10^{-5} M and 56.8% at 1×10^{-4} M. At the highest concentration (0.001 M), contraction decreased significantly to 10.1% (**Figure 5(B)**). Overall, both compounds reduced phenylephrine-induced contraction in Pulmonary artery tissue; however, F1 exhibited a much stronger and more rapid dose-dependent inhibitory effect, while F3 showed limited activity at lower concentrations and a more gradual reduction at higher doses.

Influence of nitric oxide synthase blockade on F1 and F3 activity

The effects of F1 and F3 on Pulmonary artery contraction were evaluated under potassium chloride (15 μM)-induced conditions in the presence of the nitric oxide synthase inhibitor L-NAME (1 μM). F1 demonstrated a strong concentration-dependent inhibitory effect on contraction. The contraction force decreased from 86% at 1×10^{-9} M to 76.4% at 1×10^{-8} M and 69.2% at 1×10^{-7} M (**Figure 6(A)**). A more pronounced reduction was observed at 1×10^{-6} M (34.1%), followed by a sharp decline to 4.2% at 1×10^{-5} M. Complete inhibition (0%) was achieved at 1×10^{-4} M and maintained at 0.001 M. The IC_{50} value for F1 was 4.12×10^{-7} M. In contrast, F3 showed a more gradual and less potent effect. Contraction decreased from 85.1% at

1×10^{-9} M to 66.7% at 1×10^{-8} M and 49.6% at 1×10^{-7} M. Further reductions were observed at higher concentrations, reaching 48.5% at 1×10^{-6} M, 40.4% at 1×10^{-5} M, 30.3% at 1×10^{-4} M, and 22% at 0.001 M. The IC_{50} value for F3 was 8.9×10^{-8} M. Overall, both compounds reduced KCl-induced contraction in the presence of L-NAME; however, F1 exhibited a more pronounced and rapid inhibitory effect, while F3 showed a weaker and more gradual response, indicating differences in their mechanisms and potency under nitric oxide synthase inhibition.

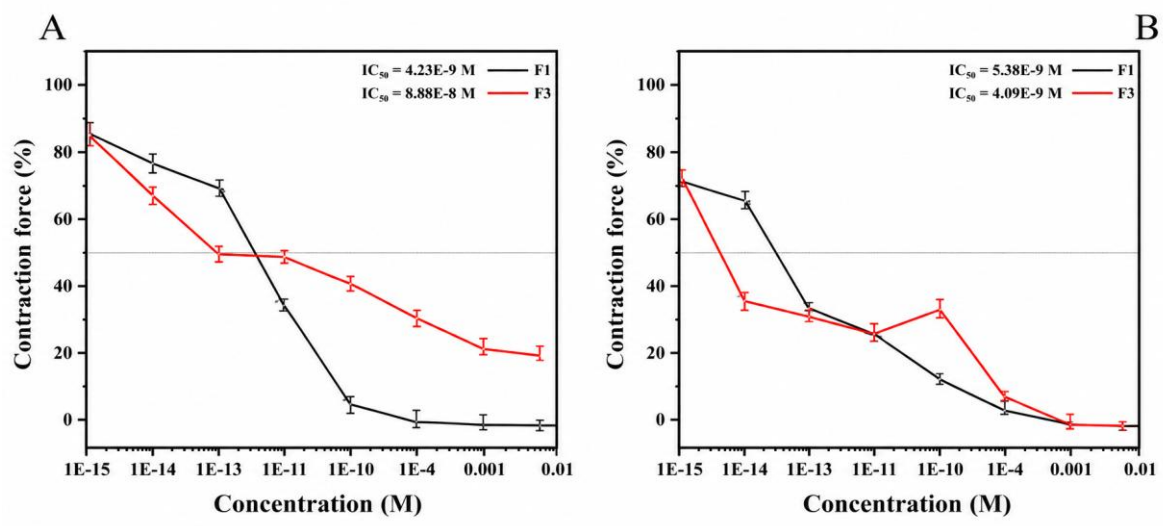


Figure 6 Effect of F1 and F3 on potassium chloride (15 μM)-induced contraction in Pulmonary artery tissue in the presence of L-NAME (1 μM) (A), Effect of F1 and F3 on phenylephrine (1 μM)-induced contraction in Pulmonary artery tissue in the presence of L-NAME (1 μM).

The effects of F1 and F3 on phenylephrine (1 μM)-induced contraction in Pulmonary artery tissue were evaluated in the presence of the nitric oxide synthase inhibitor L-NAME (1 μM). Under these conditions, F1 demonstrated a clear concentration-dependent decrease in contraction force. The response declined from 71.5% at 1×10^{-9} M to 66.3% at 1×10^{-8} M, followed by a sharper reduction to 32.9% at 1×10^{-7} M and 25.6% at 1×10^{-6} M (**Figure 6(B)**). At higher concentrations, contraction further decreased to 12.5% at 1×10^{-5} M and 4.3% at 1×10^{-4} M, reaching complete relaxation (0%) at 0.001 M. The IC_{50} value for F1 was 3.88×10^{-8} M. F3 also reduced contraction in a dose-dependent manner, although with slight variability at intermediate concentrations. The contraction dropped from 75.3% at 1×10^{-9} M to 35.1% at 1×10^{-8} M and 30.8% at 1×10^{-7} M, then further to 25.47% at 1×10^{-6} M. A moderate increase to 33% was observed at 1×10^{-5} M, followed by a marked decrease to 8.3% at 1×10^{-4} M and complete inhibition (0%) at 0.001 M. The IC_{50} value for F3 was 4.586×10^{-9} M. Overall, both F1 and F3 retained their vasorelaxant effects in the presence of L-NAME, suggesting that their mechanisms of action are at least partially independent of nitric oxide pathways.

In silico molecular docking studies of *F1 and F3* compounds targeting Ca^{2+} ion channels

In this study, L-type (Cav1.2) and R-type (Cav2.3) calcium channels were selected for molecular docking analysis due to their critical roles in regulating vascular smooth muscle function. L-type calcium channels are the primary pathways for Ca^{2+} influx in vascular smooth muscle cells and are directly responsible for initiating and maintaining contractile responses in both aortic and pulmonary arteries [22]. Therefore, modulation of these channels is considered a key mechanism underlying vasorelaxation and the regulation of vascular tone. In addition, R-type calcium channels were included to evaluate the possible involvement of alternative calcium entry pathways in vascular smooth muscle activity. Although their contribution is less dominant compared to L-type channels, R-type channels may participate in fine regulation of calcium homeostasis and cellular excitability [23]. The combined analysis of these 2

channel types allowed a more comprehensive assessment of the interaction between the studied compounds (F-1 and F-3) and calcium-dependent mechanisms, providing deeper insight into their potential pharmacological effects on vascular smooth muscle [24].

Table 4 Binding energies and predicted inhibitory constants (Ki) of F1 and F3 against calcium-regulating proteins based on molecular docking.

Channels	Ligands	Binding energy Kkal/mol	Estimated Ki value μM
Ca^{2+} L type channel	F1	−8.1	1.142
	F3	−8.2	0.964
Ca^{2+} R type channel	F1	−8.0	1.35
	F3	−7.7	2.245
Ca^{2+}-ATPases (calcium ATPases)	F1	−8.8	0.35
	F3	−8.5	0.581
NCX1	F1	−7.0	7.324
	F3	−7.8	1.896
RyR2	F1	−6.6	14.39
	F3	−6.5	17.04

Note: The Ki values were calculated from docking-derived binding energies and represent predicted estimates. These values should be interpreted with caution, as molecular docking does not fully account for dynamic biological conditions.

Ca^{2+} L type channel

Regulation of vascular tone is a fundamental physiological process that ensures proper blood flow and pressure within the cardiovascular system. This process is mainly controlled by vascular smooth muscle cells, where calcium ions play a central role in mediating contraction and relaxation. Among the various calcium entry pathways, L-type voltage-gated calcium channels are considered the primary route for calcium influx in vascular smooth muscle, particularly in the aorta and pulmonary artery. Activation of these channels leads to an increase in intracellular calcium concentration, which ultimately triggers muscle contraction [25]. Dysregulation of calcium homeostasis is closely associated with the development of cardiovascular disorders, including hypertension and pulmonary arterial hypertension. Therefore, calcium channels, especially L-type channels, are regarded as important pharmacological targets for the development of new therapeutic agents aimed at modulating vascular tone. In addition to L-type channels, other calcium channels, such as R-type channels, may contribute to the fine regulation of calcium dynamics in vascular tissues, although their role is less pronounced. In recent years, considerable attention has been given to the study of biologically active compounds that can influence vascular function through interactions with calcium channels. Compounds with phenolic and isoquinoline structures have demonstrated promising biological activities, including vasorelaxant effects and potential cardiovascular benefits. In this context, the present study focuses on 2 biologically active compounds, F-1 and F-3, and their effects on vascular smooth muscle [26,28]. Their pharmacological activity was evaluated using a combination of *in vitro* experiments on isolated aortic and pulmonary artery tissues, *in vivo* studies, and *in silico* molecular docking approaches. This integrated methodology allows for a comprehensive assessment of their potential mechanisms of action. The aim of this study was to investigate the effects of F-1 and F-3 on vascular smooth muscle and to determine their possible interaction with L-type and R-type calcium channels, providing insight into their pharmacological potential [29,32].

The molecule 1-phenyl-6,7-dimethoxy-1,2,3,4-tetrahydroisoquinoline hydrochloride (F-1) demonstrates complex interactions with the active site of the L-type calcium channel Cav1.2 at the coordinates

center_x = 168.279698, center_y = 176.439484, and center_z = 180.397000 (**Figure 7(a)**). The binding energy of the complex was calculated to be −8.1 kcal/mol, indicating a high affinity of the ligand for the active site. Based on this binding energy, the predicted inhibition potency was determined to be approximately 1.142 μM, suggesting a moderate inhibitory potential of the compound toward the target protein. The amino acid residues are involved in various types of non-covalent interactions. ASN F: 395 forms a classical hydrogen bond with the hydroxyl group of the ligand through its amide side chain. GLU A 591 participates in hydrogen bonding, as its acidic groups can interact with polar hydrogen atoms of the ligand, thereby enhancing electrostatic stabilization of the complex. TYR A 1035 forms a carbonyl hydrogen bond with the oxygen atoms of the ligand, helping to fix it in an optimal orientation. ASP A 598 interacts with the aromatic ring of the ligand through a π-anion interaction, resulting from the attraction between the negatively charged COO^- group and the π-electron system of the ligand. TYR F 396 participates in π-alkyl interactions, providing additional hydrophobic stabilization. LEU F 269 forms an unfavorable donor–donor interaction, causing slight steric repulsion; however, the overall interaction network maintains the stability of the complex (**Figure 9(c)**).

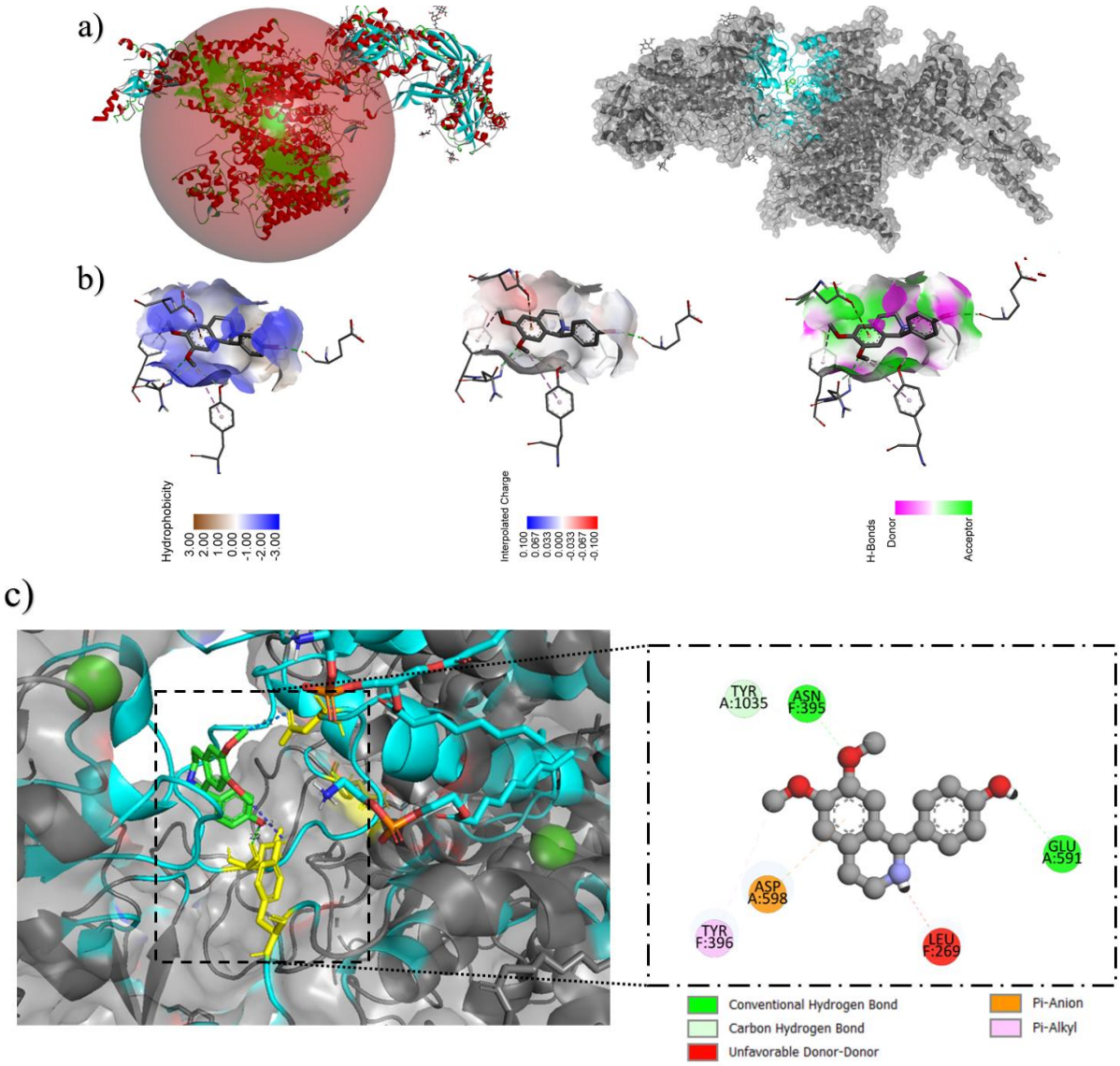
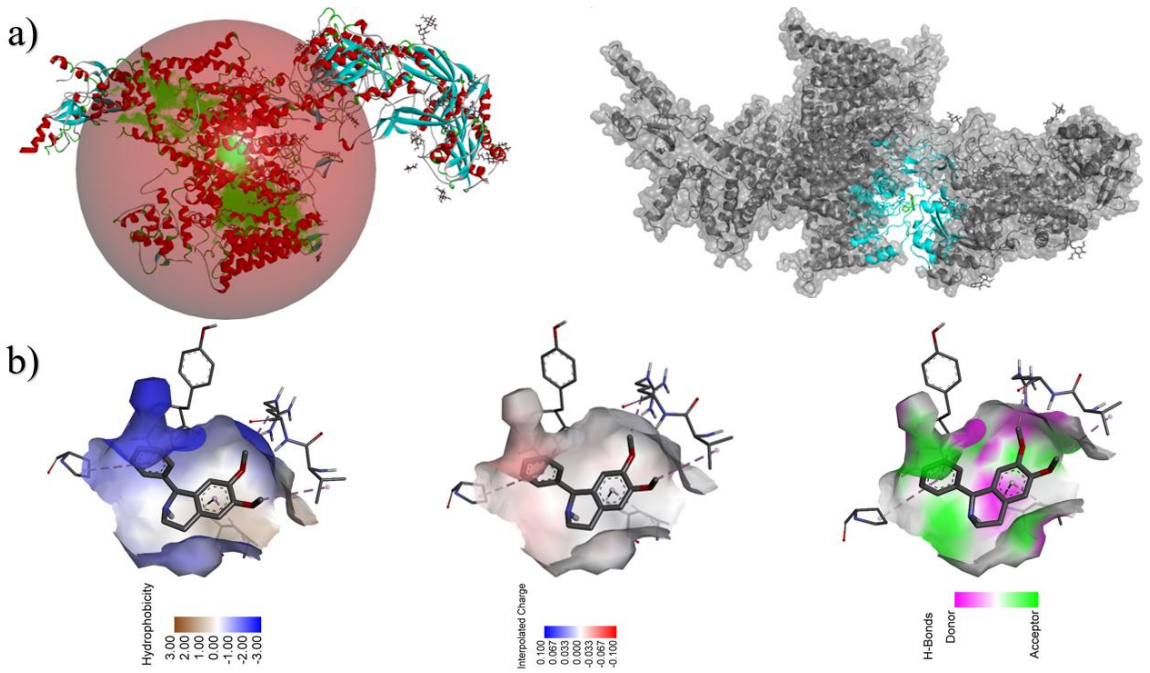


Figure 7 Molecular docking analysis of F1 with the L-type Ca^{2+} channel. (a) Localization of the active binding site within the channel structure; (b) Detailed ligand–receptor interaction profile illustrating key binding interactions; (c) Binding conformations of F1 within sites 2 and 3 of the channel structure.

Within the framework of the present study, molecular docking analysis was performed to investigate the interaction between 1-(4-hydroxyphenyl)-6,7-dimethoxy-1,2,3,4-tetrahydroiso-quinoline hydrochloride (F-3) and the voltage-dependent L-type calcium channel (Cav1.2). The active site of the protein was determined using Discovery Studio software. Based on the obtained data, the docking grid coordinates were defined as follows: center_x = 168.279698, center_y = 176.439484, and center_z = 180.397000 (**Figure 8(a)**), corresponding to the functionally relevant region of the channel. The molecular docking results demonstrated that F-3 binds within the active site of Cav1.2 with a binding energy of −8.2 kcal/mol (**Figure 9(b)**). This value indicates moderate and favorable binding of the ligand to the target protein, rather than definitive high-affinity binding or confirmed functional inhibition. Based on the calculated binding energy, the predicted inhibition constant was approximately 0.964 μM. Interaction analysis showed that the F-3 molecule forms a complex with the protein through several non-covalent interactions. In particular, amino acid residues VAL A 592, ARG A 593, and PRO A 75 participate in alkyl interactions. These docking results suggest a potential interaction between F-3 and Cav1.2; however, they should be interpreted as supportive *in silico* evidence and do not independently confirm functional inhibition of the calcium channel without experimental validation. and π-alkyl interactions, contributing to the stabilization of the ligand within the hydrophobic region of the active site. The residue TYR A 585 forms a π–π stacking interaction with the aromatic system of the ligand, further enhancing binding affinity. Additionally, LEU F 269 participates in a π-donor hydrogen interaction, contributing to the proper orientation of the ligand within the binding pocket. The ASP A 586 residue interacts with the ligand through van der Waals forces, providing additional stabilization of the complex (**Figure 8(c)**). Thus, the obtained results indicate that compound F-3 is capable of effectively interacting with the active site of the L-type calcium channel through a combination of hydrophobic, π–π, and hydrogen interactions. The relatively low Ki value (0.964 μM) together with the favorable binding energy (−8.2 kcal/mol) suggests that F-1 has a strong inhibitory potential and may effectively modulate the activity of the Cav1.2 channel, making it a promising candidate for further pharmacological investigation.



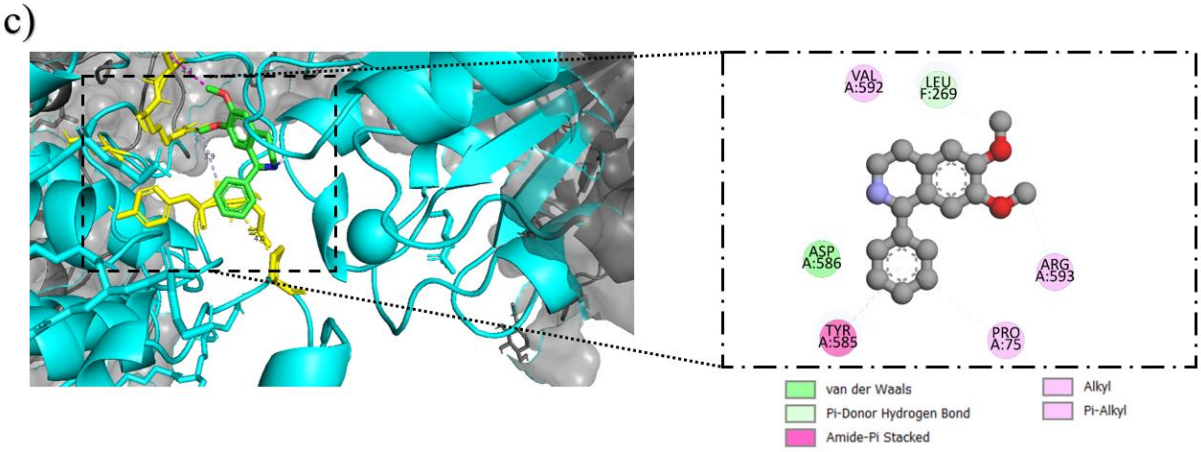
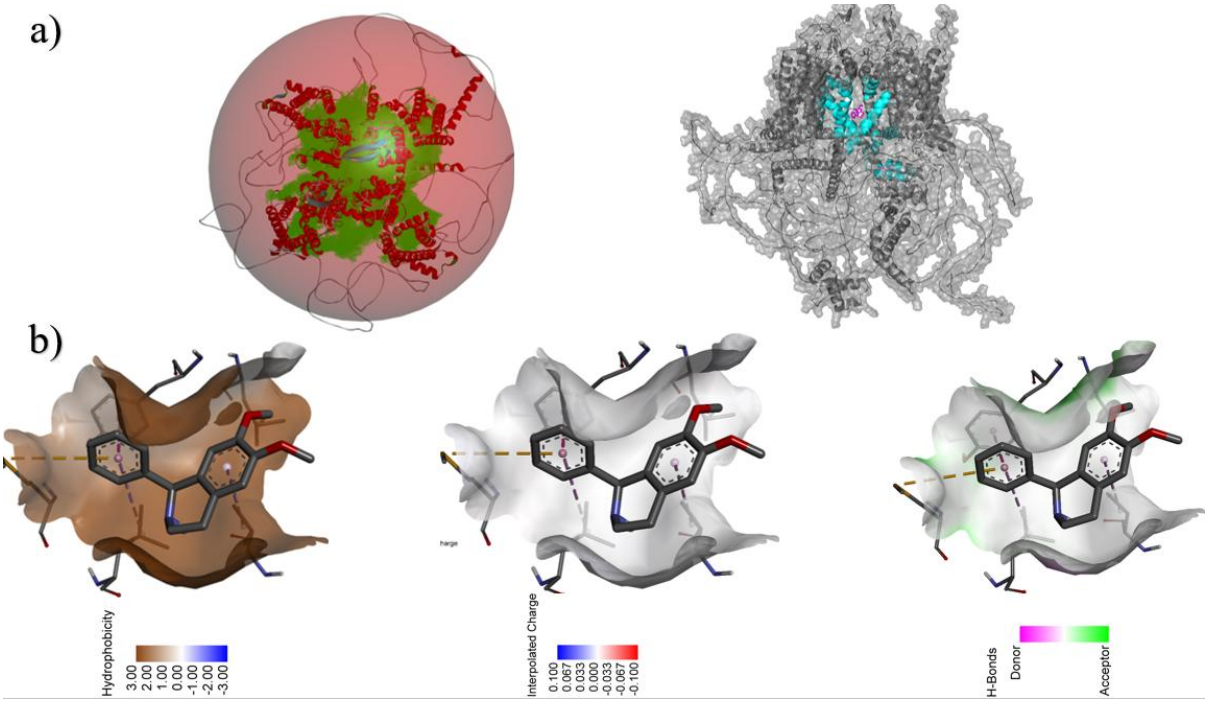


Figure 8 Molecular docking analysis of F3 with the L-type Ca^{2+} channel. (a) Localization of the active binding site within the channel structure; (b) Detailed ligand–receptor interaction profile illustrating key binding interactions; (c) Binding conformations of F3 within sites 2 and 3 of the channel structure.

Ca^{2+} R type channel

R-type calcium channels are voltage-gated calcium channels that belong to the high-voltage-activated (HVA) family and are encoded by the CACNA1E gene. These channels are also known as Cav2.3 channels and are mainly expressed in the central nervous system, particularly in the brain regions such as the cortex, hippocampus, and cerebellum [33,34]. They are also present, but at lower levels, in some peripheral tissues. These channels open in response to strong membrane depolarization and allow the influx of Ca^{2+} ions into the cell. This calcium entry plays a crucial role in regulating intracellular signaling pathways and contributes to various cellular processes. One of the main functions of R-type calcium channels is their involvement in neurotransmitter release at synapses. They are especially important in certain types of synapses where they can contribute to synaptic transmission either alone or together with other calcium channel subtypes such as P/Q-type and N-type channels. R-type calcium channels also play a role in controlling neuronal excitability and synaptic plasticity. They are involved in processes such as long-term potentiation (LTP) and long-term depression (LTD), which are fundamental mechanisms underlying learning and memory [35]. Because of their contribution to these processes, they are considered important regulators of cognitive function. Another important characteristic of R-type calcium channels is their relatively low sensitivity to many classical calcium channel blockers. For example, drugs that effectively block L-type channels, such as nifedipine or verapamil, have little effect on R-type channels. This makes them pharmacologically unique and has increased interest in developing more selective modulators targeting these channels. From a physiological and pathological perspective, R-type calcium channels are involved in several important processes. They have been associated with the modulation of pain signaling pathways, and their activity may contribute to neuropathic pain. In addition, they are implicated in neurological disorders such as epilepsy, where abnormal calcium signaling can lead to excessive neuronal excitability. There is also growing evidence that R-type channels may play a role in neurodegenerative diseases and neuroprotection mechanisms. Structurally, R-type channels consist of a large α1 subunit that forms the pore of the channel, along with auxiliary subunits that regulate channel function, trafficking, and kinetics. The α1 subunit contains voltage-sensing domains and the ion-conducting pore, which are responsible for channel activation and ion selectivity. Due to their specific expression pattern and functional importance in neuronal signaling, R-type calcium channels are considered promising targets for pharmacological and biomedical research. Understanding their structure, function, and regulation is important for developing new therapeutic strategies for neurological and cardiovascular disorders [36].

The molecular docking study demonstrated that the compound 1-phenyl-6,7-dimethoxy-1,2,3,4-tetrahydroisoquinoline hydrochloride (F-1) effectively binds to the R-type calcium channel at the active site with the coordinates (center_x = −14.791000, center_y = −8.417000, center_z = 10.185000) (**Figure 11(a)**). Analysis of intermolecular interactions revealed that hydrophobic and π-interactions play a key role in stabilizing the complex. In particular, the residue TYR A 741 participates in π–π stacking interactions with the aromatic system of the ligand. The presence of phenyl and isoquinoline fragments in the structure of F-1 facilitates efficient overlap of π-electron clouds, ensuring strong fixation of the ligand within the active site. Hydrophobic amino acid residues VAL A 401, LEU A 271, and LEU A 744 form alkyl and π-alkyl interactions with the nonpolar regions of the ligand molecule. These interactions contribute to additional stabilization of the complex through hydrophobic effects and optimal filling of the binding pocket. A significant contribution to the binding is made by the inhibitory strength toward the R-type calcium channel. residue MET A 268, which forms a π–sulfur interaction with the aromatic system of the ligand. Such interactions are important for stabilization, as the sulfur atom can effectively interact with the π-electron density of aromatic rings (**Figure 9(c)**). Thus, the binding of F-1 to the R-type calcium channel is predominantly determined by hydrophobic and π-interactions, with minimal involvement of classical hydrogen bonds, indicating that the ligand is oriented within a largely nonpolar region of the active site. The overall binding energy was calculated as −8.0 kcal/mol, suggesting that F-1 exhibits moderate and favorable interaction with the target protein and may form a relatively stable ligand–protein complex. However, this result should be considered as supportive molecular docking evidence and should not be interpreted as direct proof of functional inhibition. Based on this energy value, the predicted inhibition constant (Ki) was calculated to be approximately 1.35 μM, suggesting that F-1 exhibits a moderate



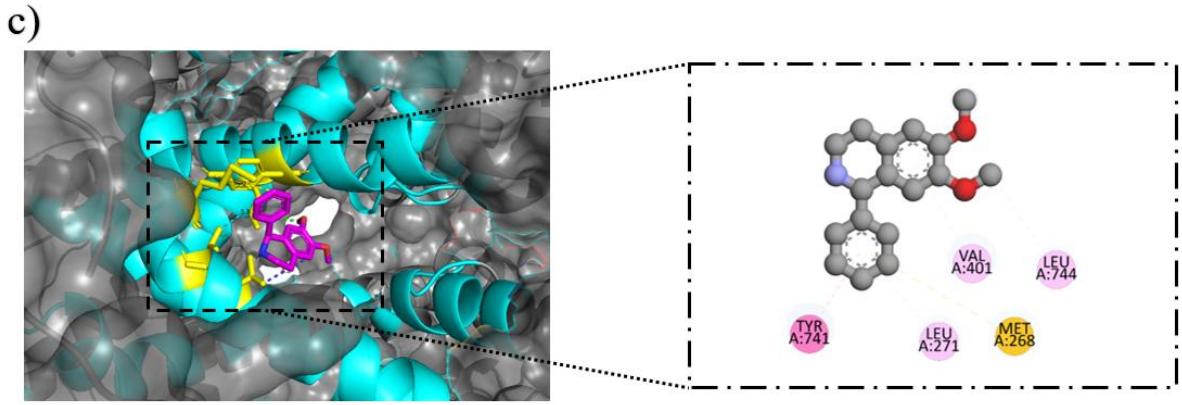


Figure 9 Molecular docking analysis of F1 with the R-type Ca^{2+} channel. (a) Localization of the active binding site within the channel structure; (b) Detailed ligand–receptor interaction profile illustrating key binding interactions; (c) Binding conformations of F1 within sites 2 and 3 of the channel structure.

Molecular docking analysis demonstrated that the compound 1-(4-hydroxyphenyl)-6,7-dimethoxy-1,2,3,4-tetrahydroisoquinoline hydrochloride (F-3) exhibits stable binding to the R-type calcium channel within the region defined by the coordinates (center x = −14.791000, center y = −8.417000, center z = 10.185000) (**Figure 11(a)**). It was established that the interaction between the ligand and the protein is predominantly governed by nonpolar contacts. The aromatic residue TYR A 741 forms a pronounced π–π interaction with the aromatic fragments of the F-3 molecule, contributing to a energetically favorable orientation of the ligand within the binding pocket. Hydrophobic amino acid residues LEU A 744, VAL A 401, and LEU A 271 also contribute to the stabilization of the complex by forming alkyl and π-alkyl interactions with the corresponding regions of the ligand. These contacts play an important role in maintaining the molecule within the hydrophobic environment of the active site. Of particular note is the residue MET A 268, which is capable of forming a π–sulfur interaction. The interaction between the sulfur-containing side chain of methionine and the π-system of the ligand further enhances the stability of the complex (**Figure 10(c)**). It should be emphasized that, despite the presence of a hydroxyl group in the structure of F-3, no hydrogen bonds are formed in this region of the active site, indicating limited accessibility of polar regions and a predominantly hydrophobic environment. The binding energy was calculated as −7.7 kcal/mol, suggesting moderate and favorable binding of the ligand to the target protein and the possible formation of a stable ligand–protein complex. However, this result should be considered as supportive docking evidence and does not necessarily confirm functional inhibition.Overall, the obtained results indicate that compound F-3 can effectively interact with this region of the R-type calcium channel through a combination of π–π, π–alkyl, and π–sulfur interactions, further supporting its potential for future pharmacological investigations.

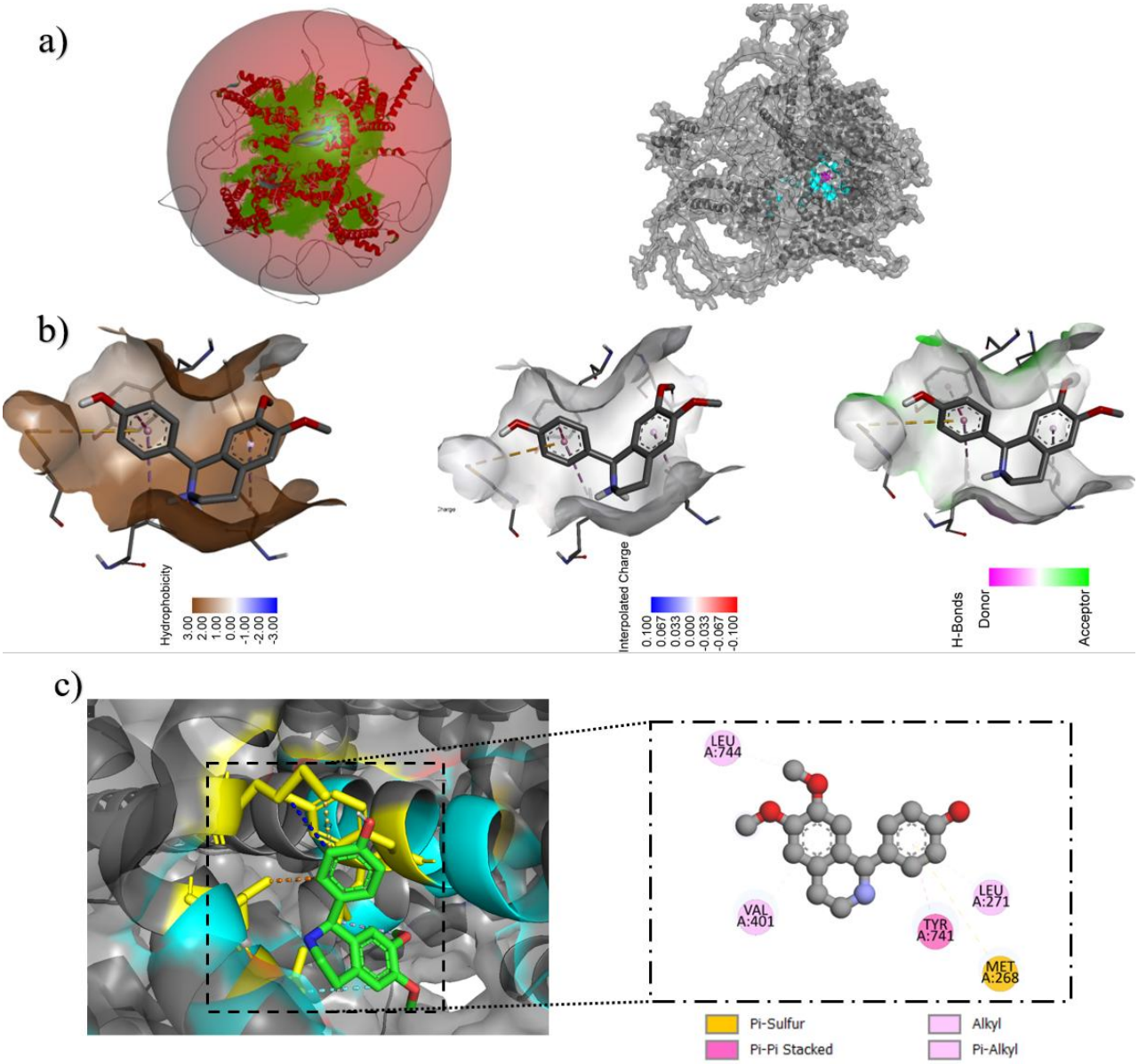


Figure 10 Molecular docking analysis of F3 with the R-type Ca^{2+} channel. (a) Localization of the active binding site within the channel structure; (b) Detailed ligand–receptor interaction profile illustrating key binding interactions; (c) Binding conformations of F3 within sites 2 and 3 of the channel structure.

Ca^{2+}-ATPases (calcium ATPases)

Ca^{2+}-ATPases are a group of membrane-bound ion pumps that play a crucial role in maintaining intracellular calcium homeostasis by actively transporting Ca^{2+} from the cytosol into intracellular stores or across the plasma membrane. These ATP-dependent transporters are essential for regulating the concentration of cytosolic calcium, which serves as a universal second messenger involved in numerous cellular processes, including contraction, proliferation, and signaling. In smooth muscle cells, precise regulation of intracellular Ca^{2+} levels is fundamental for controlling contraction and relaxation processes [37]. Smooth muscle contraction is primarily initiated by an increase in cytosolic Ca^{2+} concentration, which leads to the activation of the Ca^{2+}–calmodulin complex and subsequent stimulation of myosin light chain kinase (MLCK). This cascade ultimately results in phosphorylation of myosin light chains and the generation of contractile force. Therefore, the mechanisms responsible for Ca^{2+} removal from the cytosol are equally important for muscle relaxation and

functional balance. Among these mechanisms, Ca^{2+}-ATPases, including the sarco/endoplasmic reticulum Ca^{2+}-ATPase (SERCA) and the plasma membrane Ca^{2+}-ATPase (PMCA), play a central role. SERCA pumps Ca^{2+} from the cytosol into the sarcoplasmic reticulum, thereby reducing cytosolic Ca^{2+} concentration and promoting relaxation. Meanwhile, PMCA extrudes Ca^{2+} out of the cell, contributing to the fine-tuning of intracellular calcium levels. The coordinated activity of these pumps ensures rapid clearance of Ca^{2+} following stimulation, preventing prolonged contraction and maintaining cellular homeostasis [38]. Dysregulation of Ca^{2+}-ATPase activity in smooth muscle has been implicated in various pathological conditions, including hypertension, vascular dysfunction, and other cardiovascular diseases. Altered Ca^{2+} handling can lead to excessive contraction or impaired relaxation of vascular smooth muscle, contributing to increased vascular tone and pathological remodeling. Therefore, Ca^{2+}-ATPases represent critical targets for understanding smooth muscle physiology and for the development of therapeutic strategies aimed at modulating calcium signaling in cardiovascular and other smooth muscle-related disorders. Their functional importance highlights the need for further investigation into their regulatory mechanisms and interactions with bioactive compounds that may influence smooth muscle activity [39]. ARG A:489 residue was found to form a conventional hydrogen bond with the ligand, resulting in a binding energy of −8.8 kcal/mol, which indicates a strong and stable interaction between the compound and the target protein. Based on this binding energy, the predicted inhibition potency (Ki) was calculated to be approximately 0.35 μM, suggesting a relatively high inhibitory strength of the ligand toward the target. The docking interaction was observed within the active site defined by the coordinates (center_x = 27.060000, center_y = 1.672000, center_z = 2.679000) (**Figure 11(a)**), which correspond to the functionally significant region of the protein. This region is characterized by the presence of key amino acid residues involved in ligand recognition and binding, making it a suitable site for effective molecular interaction. The preference for interaction with ARG A:489 can be explained by the chemical nature of both the ligand and the amino acid residue. Arginine contains a positively charged guanidinium group at physiological pH, which is highly capable of forming strong electrostatic interactions and hydrogen bonds with polar functional groups of the ligand. If the ligand possesses electronegative atoms such as oxygen or nitrogen (e.g., hydroxyl, carbonyl, or methoxy groups), these groups can effectively act as hydrogen bond acceptors or donors, enabling the formation of a stable conventional hydrogen bond with the arginine side chain. Such interactions are particularly important because hydrogen bonds not only stabilize the ligand within the active site but also ensure proper orientation of the molecule in the binding pocket. In addition, the presence of a charged residue like ARG A: 489 in the binding site often indicates a functionally important region of the protein, where electrostatic interactions play a key role in ligand recognition and binding specificity (**Figure 11(c)**).

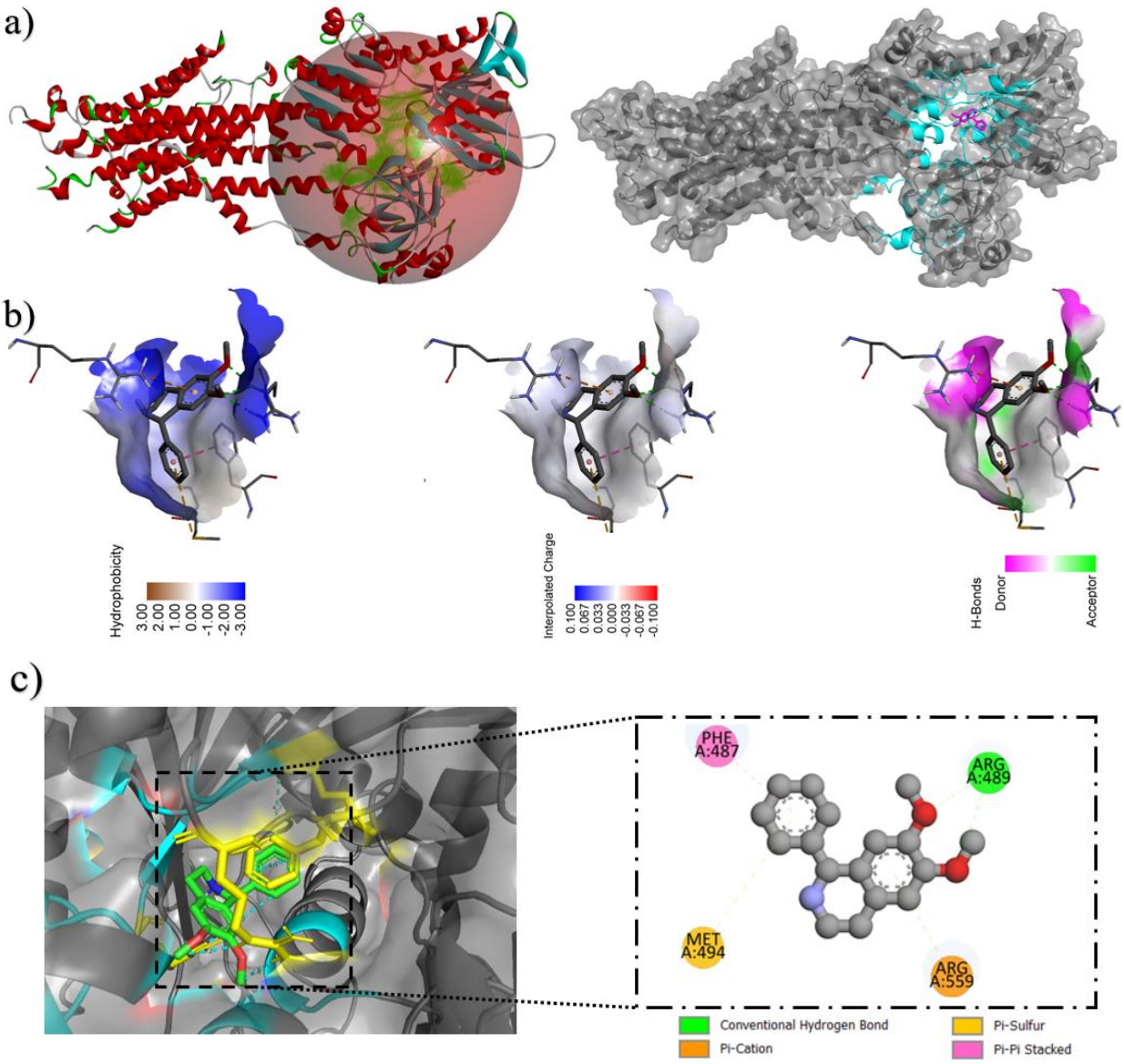


Figure 11 Molecular docking analysis of F1 with the Ca^{2+}-ATPases (calcium ATPases). (a) Localization of the active binding site within the channel structure; (b) Detailed ligand–receptor interaction profile illustrating key binding interactions; (c) Binding conformations of F1 within sites 2 and 3 of the channel structure.

The compound F-3 was docked into the same active site defined by the coordinates (center_x = 27.060000, center_y = 1.672000, center_z = 2.679000) (**Figure 12(a)**), and the results demonstrated a favorable binding affinity with a calculated binding energy of −8.5 kcal/mol, indicating stable interaction between the ligand and the target protein. Interaction analysis revealed that F-3 forms multiple types of non-covalent interactions with key amino acid residues within the binding pocket. In particular, LYS A:492 and CYS A:560 participate in conventional hydrogen bonding, which plays a crucial role in stabilizing the ligand and maintaining its proper orientation within the active site. The residue PHE A:487 is involved in π–π stacked interactions with the aromatic system of the ligand, contributing to strong π-electron cloud overlap and enhanced binding stability. Additionally, ALA A:516 and LEU A:561 participate in π-alkyl interactions, providing hydrophobic stabilization through favorable contacts between nonpolar regions of the ligand and the protein. ARG A:559 forms a π-cation interaction with the aromatic ring of the ligand (**Figure 12(c)**), further strengthening the complex through electrostatic attraction between the positively charged guanidinium

group and the π-electron system. The combination of hydrogen bonding, π–π stacking, π-alkyl, and π-cation interactions indicates that F-3 binds effectively within a mixed polar and hydrophobic environment of the active site. The binding energy of −8.5 kcal/mol suggests a relatively strong and stable ligand–protein complex, highlighting the potential of F-3 to interact efficiently with the target protein and modulate its activity.

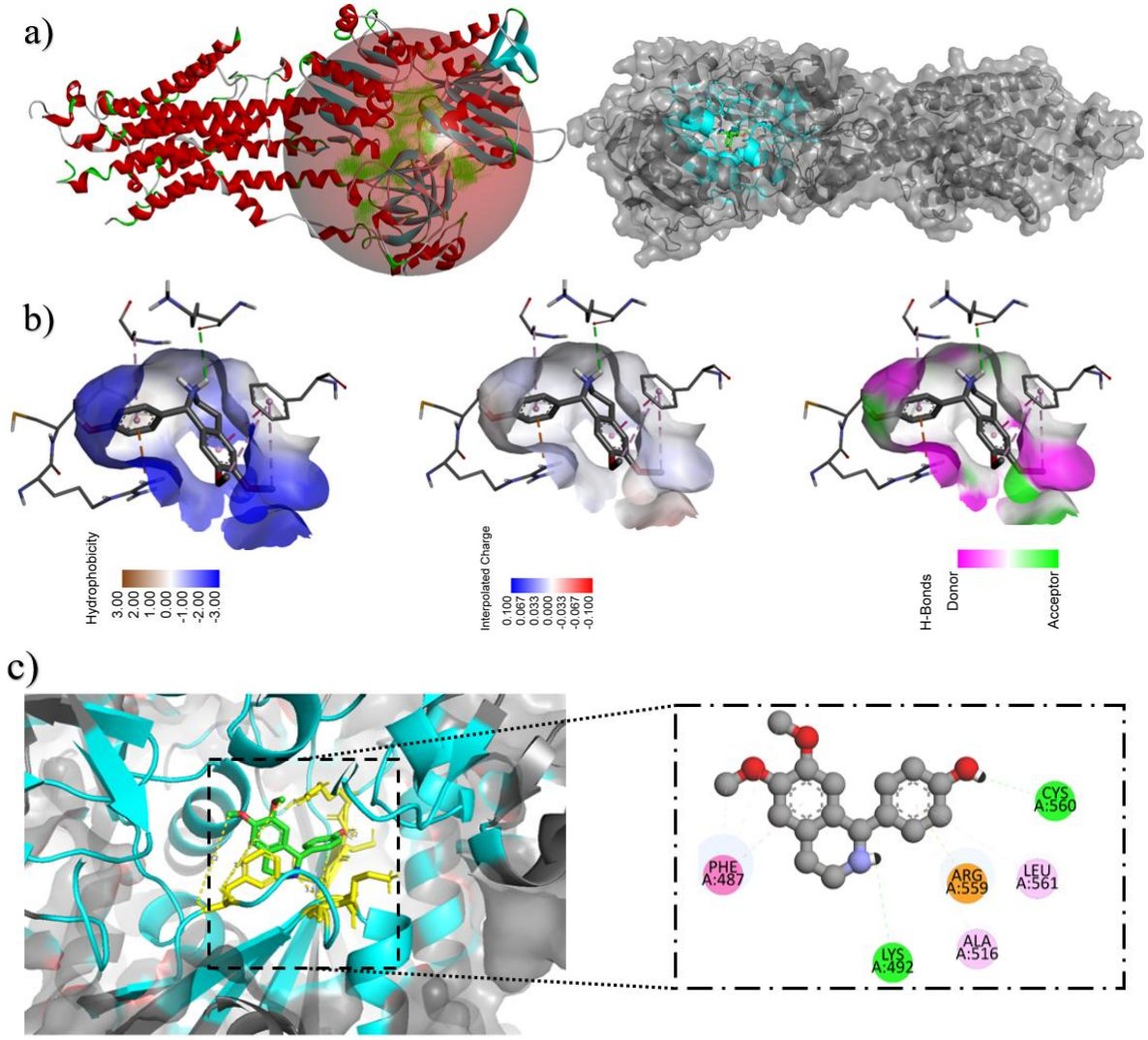


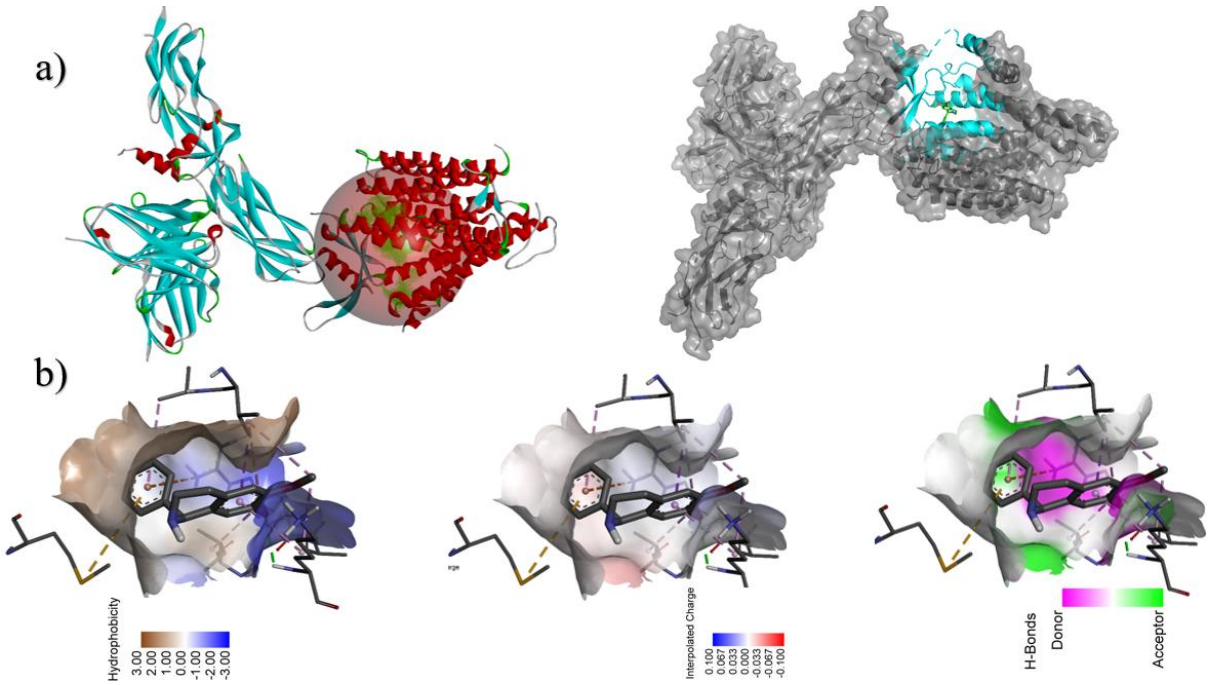
Figure 12 Molecular docking analysis of F3 with the Ca^{2+}-ATPases (calcium ATPases). (a) Localization of the active binding site within the channel structure; (b) Detailed ligand–receptor interaction profile illustrating key binding interactions; (c) Binding conformations of F3 within sites 2 and 3 of the channel structure.

NCX1

NCX1 (Na^+/Ca^{2+} exchanger 1) is a membrane transport protein that plays a crucial role in maintaining intracellular calcium (Ca^{2+}) homeostasis by exchanging intracellular Ca^{2+} for extracellular sodium (Na^+) across the plasma membrane. This exchanger operates in a reversible manner, depending on the electrochemical gradients of Na^+ and Ca^{2+}, allowing it to either extrude Ca^{2+} from the cell (forward mode) or facilitate Ca^{2+} entry under certain physiological or pathological conditions (reverse mode) [40]. In smooth muscle cells, NCX1 is particularly important for regulating intracellular Ca^{2+} concentration, which directly influences contraction and relaxation processes. An increase in cytosolic Ca^{2+} leads to smooth muscle contraction through activation of the Ca^{2+}–calmodulin–myosin light chain kinase pathway, whereas the removal of Ca^{2+} promotes relaxation. In this context, NCX1 contributes to fine-tuning vascular tone by controlling Ca^{2+} fluxes across the plasma membrane. NCX1 is widely expressed in cardiovascular tissues,

including vascular smooth muscle, where it plays a significant role in regulating vascular reactivity and blood pressure. Under physiological conditions, the exchanger helps to maintain low intracellular Ca^{2+} levels by extruding excess Ca^{2+} from the cytosol. However, under pathological conditions such as ischemia, hypoxia, or altered ion gradients, NCX1 can operate in reverse mode, leading to increased intracellular Ca^{2+} accumulation. This can result in enhanced smooth muscle contraction, vascular dysfunction, and contributes to the development of cardiovascular diseases such as hypertension. Due to its central role in calcium homeostasis and smooth muscle function, NCX1 has attracted significant attention as a potential pharmacological target. Modulation of NCX1 activity may provide therapeutic benefits in conditions associated with abnormal Ca^{2+} signaling, particularly in cardiovascular and smooth muscle-related disorders. Therefore, understanding the structure, function, and regulation of NCX1 is essential for the development of novel strategies aimed at controlling calcium dynamics in smooth muscle physiology and pathology [41].

The docking of compound F-1 into the active site defined by the coordinates (center_x = 142.026713, center_y = 158.751000, center_z = 153.700000) (**Figure 13(a)**) resulted in a binding energy of −7.0 kcal/mol, indicating the formation of a stable ligand–protein complex. Detailed interaction analysis showed that F-1 establishes several types of non-covalent interactions with key residues in the binding pocket. Among them, ARG A:232 and MET A:105 are involved in π-cation and π–sulfur interactions, respectively, which contribute significantly to the stabilization of the ligand through electrostatic and sulfur-related contacts. Hydrophobic contacts also play an important role in maintaining the complex stability. Residues ALA A:821 and ILE A:241 participate in alkyl and π-alkyl interactions, promoting favorable nonpolar interactions between the ligand and the protein. Additionally, VAL A:820 contributes through π–σ interactions, further reinforcing the hydrophobic environment within the binding site. Hydrogen bonding is observed with LYS A:235, which forms a conventional hydrogen bond and enhances the specificity and stability of the binding. Moreover, ALA A:233 is involved in a carbon–hydrogen bond, providing additional support to the overall interaction network (**Figure 13(c)**).



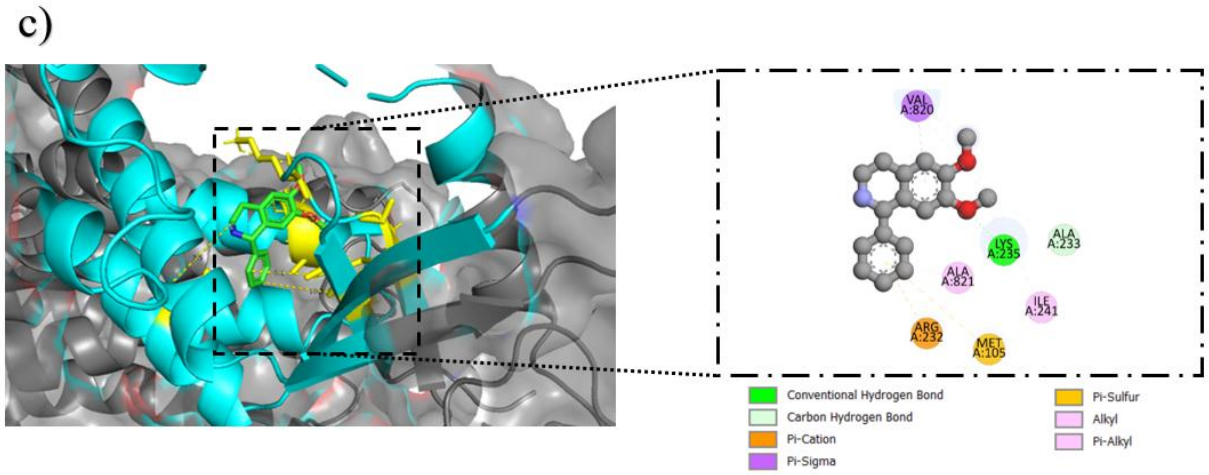


Figure 13 Molecular docking analysis of F1 with the Na^+/Ca^{2+} exchanger 1. (a) Localization of the active binding site within the channel structure; (b) Detailed ligand–receptor interaction profile illustrating key binding interactions; (c) Binding conformations of F1 within sites 2 and 3 of the channel structure.

The compound F-3 was docked into the same active site defined by the coordinates (center_x = 142.026713, center_y = 158.751000, center_z = 153.700000) (**Figure 14(a)**), resulting in a binding energy of −7.8 kcal/mol, indicating a stable and favorable interaction between the ligand and the NCX1 (Na^+/Ca^{2+} exchanger 1) protein. Interaction analysis revealed that F-3 forms several types of non-covalent interactions with key amino acid residues within the binding pocket. In particular, LEU A:102, VAL A:168, VAL A:99, and ALA A:830 (**Figure 14(c)**) participate in alkyl and π-alkyl interactions, contributing to strong hydrophobic stabilization of the ligand within the nonpolar regions of the active site. These interactions play an important role in maintaining the ligand in a well-fitted orientation. Additionally, HIS A:165 is involved in a carbon–hydrogen bond, which provides further stabilization of the complex through weak but important directional interactions. The residue ASP A:829 participates in a π-anion interaction, contributing to electrostatic attraction between the negatively charged side chain and the π-electron system of the ligand. Furthermore, GLU A:97 forms a conventional hydrogen bond, which enhances the specificity and stability of ligand binding. The combination of hydrophobic (alkyl and π-alkyl), hydrogen bonding, and electrostatic interactions indicates that F-3 is effectively accommodated within the active site of the NCX1 exchanger. The binding energy of −7.8 kcal/mol suggests a relatively strong affinity of the ligand toward the protein, highlighting its potential to interact with and modulate NCX1 activity through a well-balanced network of molecular interactions.

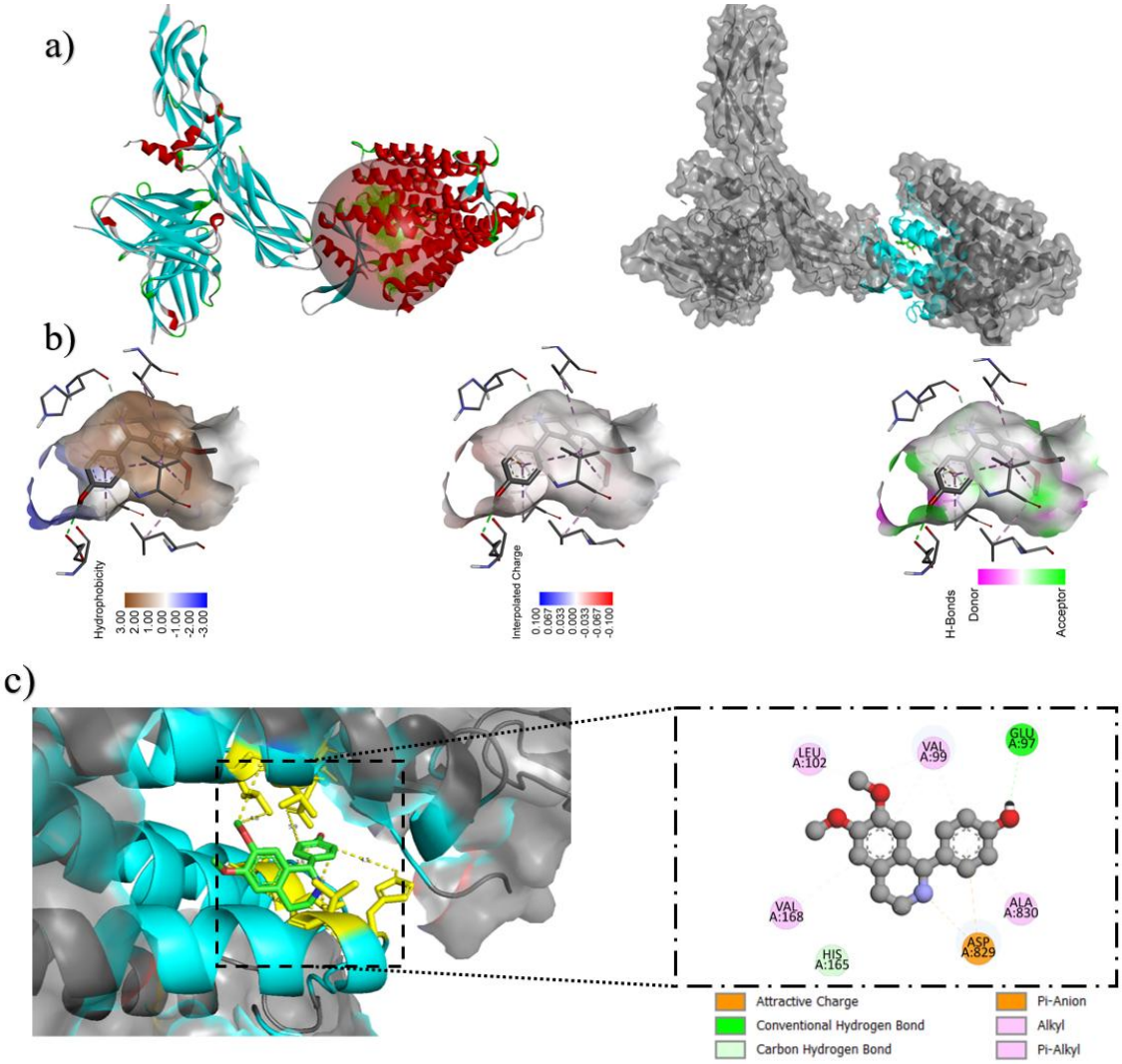


Figure 14 Molecular docking analysis of F3 with the Na^{+}/Ca^{2+} exchanger 1. (a) Localization of the active binding site within the channel structure; (b) Detailed ligand–receptor interaction profile illustrating key binding interactions; (c) Binding conformations of F3 within sites 2 and 3 of the channel structure.

RyR2

Ryanodine Receptor 2 (RyR2) is a large intracellular calcium release channel located primarily on the membrane of the sarcoplasmic reticulum in cardiac muscle cells. It plays a central role in regulating intracellular calcium (Ca^{2+}) dynamics, which are essential for excitation–contraction coupling in the heart. Upon stimulation, RyR2 mediates the rapid release of Ca^{2+} from the sarcoplasmic reticulum into the cytosol, leading to activation of the contractile machinery and subsequent cardiac muscle contraction [42]. In smooth muscle, although RyR2 is more prominently studied in cardiac tissue, its functional role is also closely related to intracellular calcium signaling. Calcium release through RyR channels contributes to localized Ca^{2+} signaling events, which can influence smooth muscle tone, contraction, and relaxation processes. These calcium "sparks" generated by RyR2 activity are important for fine-tuning cellular responses and maintaining calcium homeostasis. The activity of RyR2 is tightly regulated by various factors, including intracellular calcium levels, ATP, phosphorylation status, and interaction with accessory proteins [43]. Dysregulation of RyR2 function can lead to abnormal calcium leakage from the sarcoplasmic reticulum, resulting in disrupted calcium homeostasis. This can contribute to pathological conditions such as cardiac arrhythmias, heart failure, and altered smooth muscle function. Given its crucial role in calcium signaling, RyR2 represents an important pharmacological target.

Modulating its activity can influence intracellular calcium levels and, consequently, muscle contractility. Therefore, understanding the structure and function of RyR2 is essential for developing therapeutic strategies aimed at regulating calcium-dependent processes in both cardiac and smooth muscle physiology [44].

The compound F-1 was docked into the active site of the Ryanodine Receptor 1 (RyR2) defined by the coordinates (center_x = 9.181367, center_y = 17.019000, center_z = 27.203000) (**Figure 15(a)**), and the results showed a binding energy of −6.6 kcal/mol, indicating a moderate level of interaction between the ligand and the receptor. Interaction analysis revealed that F-1 forms key non-covalent interactions with amino acid residues within the binding pocket. In particular, GLU A:701 and GLU A:711 participate in π-anion interactions, which are driven by electrostatic attraction between the negatively charged carboxylate groups of glutamic acid and the π-electron system of the ligand. These interactions contribute to the stabilization of the ligand within the active site. Additionally, TYR B:703 is involved in π-alkyl interactions, which provide hydrophobic stabilization through favorable contacts between the aromatic system of the ligand and the nonpolar regions of the tyrosine residue (**Figure 15(c)**). Such interactions help to anchor the ligand in a proper orientation within the binding pocket.

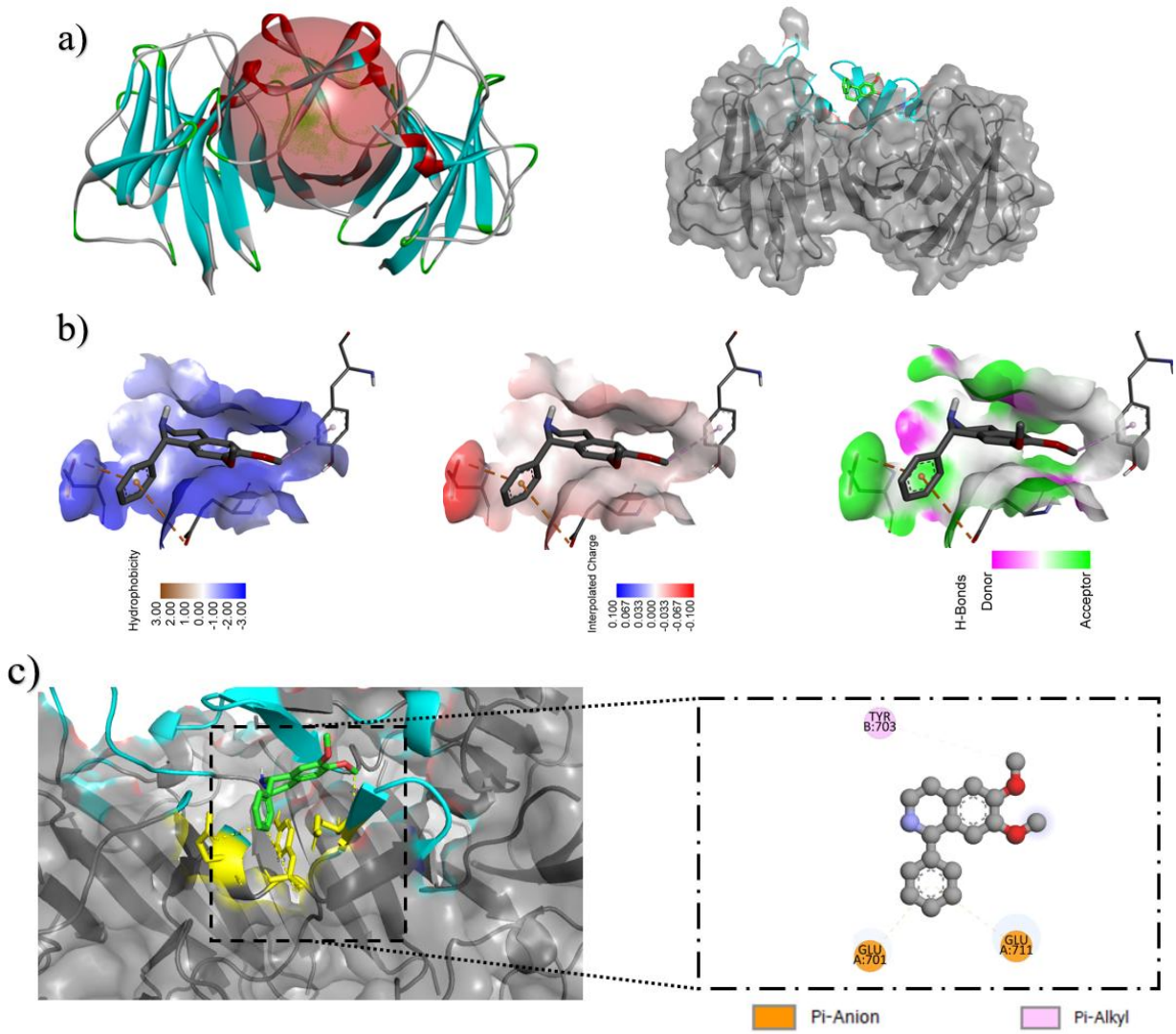


Figure 15 Molecular docking analysis of F1 with the RyR2. (a) Localization of the active binding site within the channel structure; (b) Detailed ligand–receptor interaction profile illustrating key binding interactions; (c) Binding conformations of F1 within sites 2 and 3 of the channel structure.

The compound F-3 was docked into the active site of the Ryanodine Receptor 1 (RyR2) defined by the coordinates (center_x = 9.181367, center_y = 17.019000, center_z = 27.203000), resulting in a binding energy of −6.5 kcal/mol, indicating a stable and favorable interaction between the ligand and the receptor. Interaction analysis showed that F-3 forms several types of non-covalent interactions with key amino acid residues within the binding pocket. In particular, TYR B:703 participates in π-alkyl interactions, contributing to hydrophobic stabilization through favorable contacts between the aromatic system of the ligand and the nonpolar region of the tyrosine residue. GLU A:701 is involved in multiple interactions, including π-anion, attractive charge, and conventional hydrogen bonding, which collectively enhance electrostatic stabilization and strengthen ligand binding within the active site. Additionally, GLU A:711 forms a carbon–hydrogen bond with the ligand, providing further stabilization and supporting proper ligand orientation.

Effect of A51 compound on blood pressure *in vivo* studies

The study utilized white outbred laboratory rats of both sexes (♂/♀) with a body weight of 200 ± 18.9 g. The animals were maintained under controlled environmental conditions, including a room temperature of +20 ± 5 °C, relative humidity of 75 ± 10%, and a 12:12-hour light/dark cycle, with free access to standard feed and water. Arterial blood pressure in the rats was recorded using a standard non-invasive method on the tail artery with the experimental device “Systola” (“Neurobotics”, Russia) [45]. The obtained data were analyzed using the specialized software “AcqKnowledge 4.2 for MP150” (**Figure 4**). Thus, during the experiments, in rats under physiological normal conditions, the mean values of systolic and diastolic arterial blood pressure remained practically stable over a period of 180 min. In the experimental groups, the administration of 3 different doses of compounds F-1 and F-3 resulted in the maintenance of arterial blood pressure (SBP and DBP) within the physiological norm. In the experimental group, 30 min after the injection of adrenaline hydrochloride (0.25 mg/kg), which induced a sustained model of experimental hypertension (persisting for 180 min), the animals received a single intravenous administration of compounds F-1 and F-3 at doses of 10 - 25 and 50 mg/kg. It has also been noted that arterial blood pressure (systolic and diastolic) in laboratory rats depends on physiological age-related periods. The results of the antihypertensive activity of compounds F-1 and F-3 are presented in **Figures 12** and **13**.

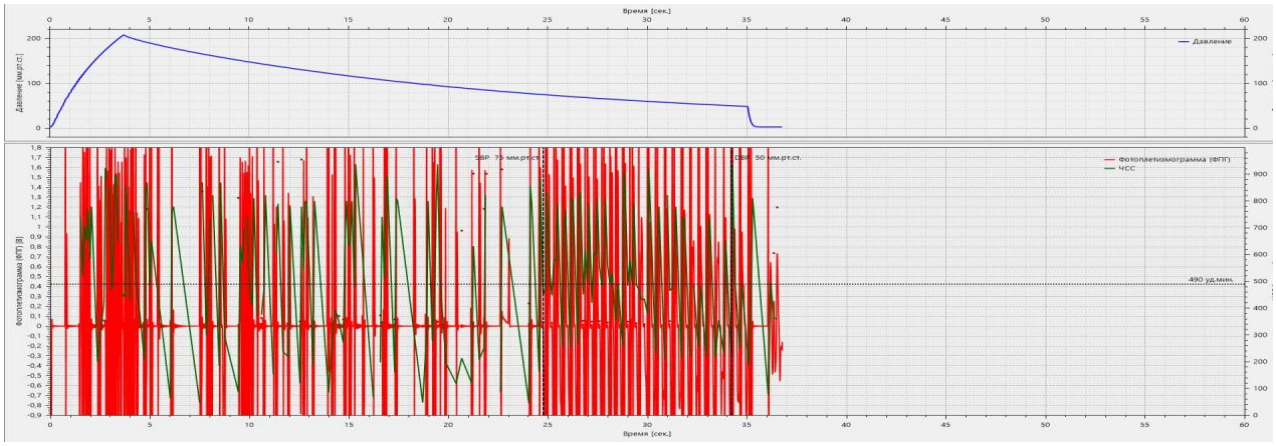


Figure 16 Original systolic recordings obtained using the Neurobotics software. (These results were used as sample datafor statistical analysis).

Systolic blood pressure

The effect of F1 on systolic arterial pressure was evaluated in adrenaline-induced hypertensive rats at doses of 10, 25, and 50 mg/kg. In the control group, baseline systolic pressure was 119.0 ± 11.8 mmHg. After adrenaline administration, systolic pressure increased to 137.5 ± 13.4 mmHg at 30 min and remained elevated during the observation period, reaching 147.5

± 13.8 mmHg at 1 h, 156.0 ± 14.9 mmHg at 2 h, 145.5 ± 14.3 mmHg at 3 h, and 131.5 ± 12.7 mmHg at 4 h. In the F1-treated groups, adrenaline administration also produced an initial increase in systolic pressure. At 30 min, systolic pressure reached 145.5 ± 13.7, 163.5 ± 16.1 and 153.5 ± 15.1 mmHg in the 10, 25, and 50 mg/kg groups, respectively. However, F1 treatment subsequently reduced systolic pressure in a time-dependent manner. At 10 mg/kg, systolic pressure decreased from 109.5 ± 10.7 mmHg at 1 h to 100.0 ± 9.9 mmHg at 2 h, 86.5 ± 8.5 mmHg at 3 h, and 93.5 ± 9.1 mmHg at 4 h. At 25 mg/kg, systolic pressure decreased from 127.5 ± 12.5 mmHg at 1 h to 111.0 ± 11.0 mmHg at 2 h, 103.0 ± 10.0 mmHg at 3 h, and 98.0 ± 9.7 mmHg at 4 h. At 50 mg/kg, F1 reduced systolic pressure from 132.5 ± 13.1 mmHg at 1 h to 128.5 ± 12.5 mmHg at 2 h, 122.5 ± 12.1 mmHg at 3 h, and 107.5 ± 10.5 mmHg at 4 h. (**Figure 17(A)**).

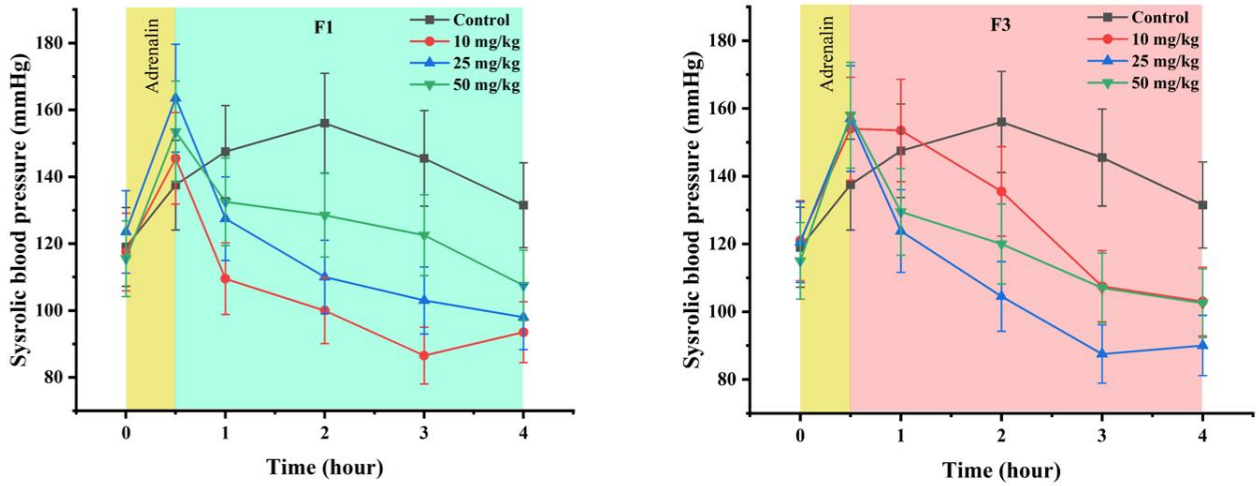


Figure 17 Effect of F1 (A) and F3 (B) on adrenaline-induced changes in systolic blood pressure *in vivo*.

The effect of F3 on systolic arterial pressure was evaluated in adrenaline-induced hypertensive rats at doses of 10, 25, and 50 mg/kg. In the control group, baseline systolic pressure was 119.0 ± 11.8 mmHg (**Figure 17**). After adrenaline administration, systolic pressure increased markedly to 137.5 ± 13.4 mmHg at 30 min and remained elevated during the observation period, reaching 147.5 ± 13.8 mmHg at 1 h, 156.0 ± 14.9 mmHg at 2 h, 145.5 ± 13.8 mmHg at 3 h, and 131.5 ± 12.7 mmHg at 4 h. In the F3-treated groups, adrenaline also caused an initial increase in systolic pressure. At 30 min, systolic pressure reached 154.0 ± 15.2, 157.0 ± 15.6, and 158.0 ± 15.6 mmHg in the 10, 25, and 50 mg/kg groups, respectively. However, subsequent administration of F3 resulted in a gradual reduction of systolic pressure over time. At 10 mg/kg, systolic pressure decreased from 153.5 ± 15.1 mmHg at 1 h to 135.5 ± 13.2 mmHg at 2 h, 107.5 ± 10.5 mmHg at 3 h, and 103.0 ± 10.1 mmHg at 4 h. At 25 mg/kg, F3 produced a more pronounced antihypertensive effect, reducing systolic pressure from 123.8 ± 12.2 mmHg at 1 h to 104.5 ± 10.3 mmHg at 2 h, 87.5 ± 8.6 mmHg at 3 h, and 90.0 ± 8.9 mmHg at 4 h. At 50 mg/kg, systolic pressure decreased from 129.5 ± 12.8 mmHg at 1 h to 120.0 ± 11.8 mmHg at 2 h, 107.0 ± 10.3 mmHg at 3 h, and 102.5 ± 10.1 mmHg at 4 h. These results indicate that F3 effectively attenuated adrenaline-induced elevation of systolic arterial pressure in a time-dependent manner. Among the tested doses, 25 mg/kg demonstrated the most pronounced systolic blood pressure-lowering effect, particularly at 3 and 4 h, suggesting that this dose may provide the optimal antihypertensive response under the present experimental conditions.

Diastolic pressure

The *in vivo* effect of F1 on diastolic blood pressure was evaluated at doses of 10, 25, and 50 mg/kg following adrenaline-induced elevation, revealing a clear time- and dose-dependent response. At baseline (0 h), diastolic blood pressure values were 83 mmHg (10 mg/kg), 99 mmHg (25 mg/kg), and 92 mmHg (50

mg/kg). After adrenaline administration (0.5 h), a significant increase was observed in all groups, reaching 106, 132, and 118 mmHg, respectively. Following this peak, F1 treatment led to a progressive decrease in diastolic blood pressure. At 1 h, the values declined to 89.5 mmHg (10 mg/kg), 93 mmHg (25 mg/kg), and 96 mmHg (50 mg/kg). At 2 h, further reductions were noted, with pressures of 80, 88, and 104 mmHg, respectively. The lowest values were recorded at 3 h, particularly in the 10 mg/kg group (65 mmHg), compared to 73and 97 mmHg in the 25 and 50 mg/kg groups. By 4 h, diastolic pressure showed slight stabilization, reaching 70 mmHg (10 mg/kg), 78 mmHg (25 mg/kg), and 93.5 mmHg (50 mg/kg) (**Figure 18(A)**).

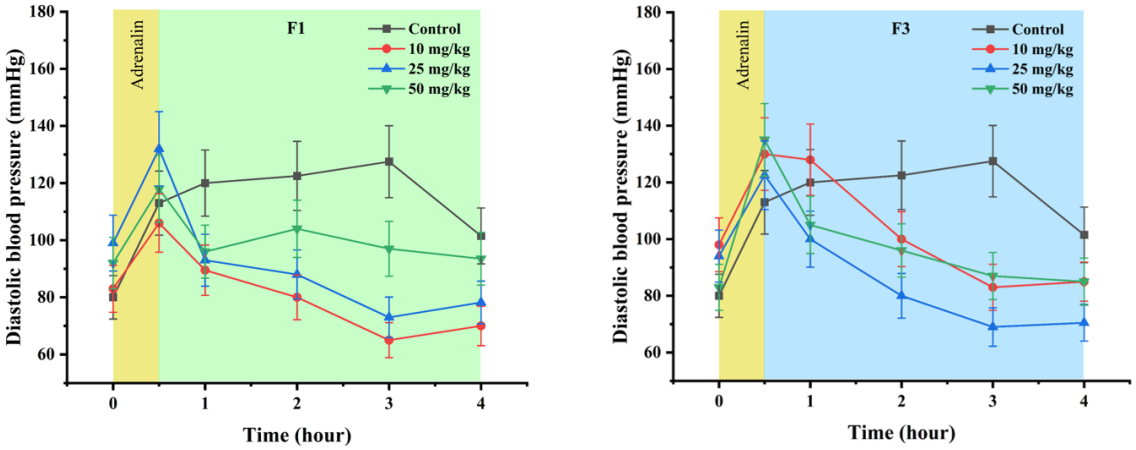


Figure 18 Effect of F1 (A) and F3 (B) on adrenaline-induced changes in diastolic blood pressure *in vivo*.

The *in vivo* effect of F3 on diastolic blood pressure was investigated at doses of 10, 25, and 50 mg/kg following adrenaline-induced elevation, demonstrating a gradual and dose-related antihypertensive response. At baseline (0 h), diastolic blood pressure values were 98 mmHg (10 mg/kg), 94 mmHg (25 mg/kg), and 83 mmHg (50 mg/kg). After adrenaline administration (0.5 h), a marked increase was observed in all groups, reaching 130, 122.5, and 135 mmHg, respectively. Following this peak, F3 induced a progressive decrease in diastolic blood pressure over time. At 1 hour, values declined to 128 mmHg (10 mg/kg), 100 mmHg (25 mg/kg), and 105 mmHg (50 mg/kg). At 2 h, further reductions were noted, with pressures of 100, 80, and 96 mmHg, respectively. The lowest levels were observed at 3 h, particularly in the 25 mg/kg group (69 mmHg), compared to 83 and 87 mmHg in the 10 and 50 mg/kg groups. By 4 h, diastolic pressure slightly stabilized at 85 mmHg (10 mg/kg), 70.5 mmHg (25 mg/kg), and 85 mmHg (50 mg/kg).

Discussion

The present study provides a comprehensive evaluation of the vasomodulatory and antihypertensive effects of compounds F1 and F3 through an integrated approach combining *in silico*, *in vitro*, and *in vivo* methodologies. The obtained results collectively demonstrate that these compounds exert their biological activity via multiple mechanisms, including modulation of adrenergic signaling, inhibition of calcium-dependent pathways, and partial involvement of nitric oxide (NO)-mediated mechanisms. Molecular docking analysis revealed that both F1 and F3 exhibit strong and stable interactions with the RyR2 receptor, a key regulator of intracellular calcium release. The binding energies of −6.6 kcal/mol (F1) and −6.5 kcal/mol (F3), along with interactions involving residues such as GLU A:701, GLU A:711, and TYR B:703, indicate favorable ligand–protein binding. These interactions, including π-anion, π-alkyl, hydrogen bonding, and electrostatic contacts, suggest that both compounds may directly influence calcium homeostasis, thereby contributing to the regulation of vascular smooth muscle tone. Functional *in vitro* experiments further confirmed the vasomodulatory potential of these compounds. F-1

exhibited a stronger inhibitory effect on phenylephrine-induced contraction than F-3, as evidenced by its lower IC_{50} value (3.1×10^{-7} vs. 4.29×10^{-6} M). This indicates that F-1 was more potent under phenylephrine-induced contraction conditions. This difference may be associated with a stronger influence of F-1 on receptor-mediated contractile mechanisms, including receptor-operated Ca^{2+} entry and intracellular Ca^{2+} mobilization, which play important roles in phenylephrine-induced vascular contraction. The gradual, concentration-dependent reduction in contraction observed with F1 suggests a more stable pharmacological profile, whereas F3 demonstrated weaker effects at low concentrations but a pronounced inhibitory response at higher doses. Mechanistically, both compounds demonstrated modulatory effects on adrenergic and calcium signaling pathways. The partial reversal of phentolamine-induced inhibition by F1 and F3 indicates that these compounds may influence α-adrenergic receptor-mediated signaling or downstream contractile mechanisms. Additionally, the observed synergistic effect with verapamil suggests that F1 and F3 enhance L-type calcium channel blockade, leading to reduced Ca^{2+} influx into vascular smooth muscle cells, which is a critical determinant of muscle contraction. The role of nitric oxide in mediating these effects was confirmed using L-NAME. The reduction in potency of both F1 and F3 in the presence of NO synthase inhibition indicates that their vasorelaxant activity is at least partially dependent on NO signaling. However, the persistence of inhibitory effects suggests that additional NO-independent pathways are also involved. Importantly, the *in vivo* experiments provide strong translational support for the observed *in vitro* findings. In adrenaline-induced hypertensive rats, both F1 and F3 effectively reduced systolic and diastolic blood pressure in a time- and dose-dependent manner. Following the administration of adrenaline hydrochloride (25 mg/kg), a sustained elevation in arterial blood pressure was observed, which served as a reliable experimental model of hypertension. Treatment with F1 and F3 at doses of 10, 25, and 50 mg/kg resulted in a progressive normalization of blood pressure values over a 4-hour period. F1 demonstrated a particularly strong antihypertensive effect, with systolic blood pressure decreasing from elevated levels (~163.5 mmHg after adrenaline) to near physiological values (as low as 86.5 mmHg at 3 h for the 10 mg/kg group). A similar trend was observed for diastolic pressure, where F1 reduced values from 132 to as low as 65 mmHg. These results highlight the rapid and effective antihypertensive action of F1, especially at lower doses. F3 also exhibited significant antihypertensive activity, although its effects were slightly less pronounced compared to F1. Nevertheless, F3 effectively reduced both systolic and diastolic blood pressure across all tested doses, indicating its potential as a vasorelaxant agent. The gradual reduction and stabilization of blood pressure observed in both compounds suggest sustained pharmacological activity without causing excessive hypotension. Taken together, the *in vivo* findings corroborate the *in vitro* and *in silico* results, demonstrating that F1 and F3 exert their antihypertensive effects through a combination of mechanisms, including inhibition of calcium influx, modulation of adrenergic signaling, and partial dependence on nitric oxide pathways. The consistent dose- and time-dependent responses further support the pharmacological relevance of these compounds. Overall, F1 emerges as the more potent and effective compound, exhibiting stronger binding affinity, higher inhibitory activity in vascular assays, and superior antihypertensive effects *in vivo*. These properties make F1 a promising candidate for further development as a therapeutic agent targeting hypertension and vascular dysfunction. Future studies should focus on detailed pharmacokinetic profiling, toxicity assessment, and structural optimization to enhance efficacy and safety. Although the present study provides integrated *in silico*, *in vitro*, and *in vivo* evidence supporting the vasomodulatory and antihypertensive effects of F1 and F3, several limitations should be acknowledged. First, although the findings suggest that the vasorelaxant effects of F1 and F3 may be associated with modulation of calcium-dependent pathways, particularly L-type calcium channels and intracellular calcium handling, these mechanisms were not fully confirmed using advanced molecular and electrophysiological approaches. Therefore, further studies using patch-clamp analysis, Western blotting, gene expression profiling, and specific pathway inhibitors are required to validate the direct involvement of calcium channels and related signaling proteins. Second, molecular docking provides supportive computational evidence regarding the possible interaction of F1 and F3 with calcium-

regulating targets such as RyR2; however, docking analysis remains a predictive model and cannot fully substitute for experimental validation. Future investigations should include molecular dynamics simulations, ligand–receptor binding assays, and electrophysiological experiments to confirm the stability, specificity, and functional relevance of these predicted interactions.

Conclusions

This study demonstrates that compounds F1 and F3 possess significant vasomodulatory and antihypertensive properties, supported by integrated *in silico*, *in vitro*, and *in vivo* analyses. Molecular docking results showed strong and stable interactions of these compounds with key residues of the RyR2 receptor, suggesting their potential role in modulating intracellular calcium signaling pathways. Functional studies revealed that both compounds effectively inhibit vascular smooth muscle contraction. Overall, F1 demonstrated higher potency and a more consistent dose-dependent response in most experimental conditions; however, the relative potency of F1 and F3 appeared to be vessel- and pathway-dependent. In particular, under certain experimental conditions, such as in the presence of L-NAME in pulmonary artery preparations, F3 showed greater potency than F1. Additionally, both compounds enhanced the inhibitory effects of verapamil and partially reversed the effects of phentolamine, indicating their involvement in calcium channel modulation and adrenergic signaling pathways. *In vivo* experiments further supported these findings, demonstrating that both F1 and F3 significantly reduced adrenaline-induced elevations in systolic and diastolic blood pressure in a time- and dose-dependent manner. F1 generally produced a more pronounced antihypertensive effect, restoring blood pressure closer to physiological levels without causing excessive hypotension. Moreover, the attenuation of their effects in the presence of L-NAME indicates that nitric oxide plays a partial role in their mechanism of action, although NO-independent pathways are also involved. Overall, these findings suggest that both F1 and F3 are promising vasomodulatory compounds, with F1 showing stronger overall activity in most assays, while F3 may exhibit higher potency under specific vessel- or pathway-dependent conditions. Future studies should focus on detailed pharmacokinetic profiling, safety evaluation, and structural optimization to fully explore their clinical applicability.

Declaration of competing interest

The authors declare that they have no known competing financial interests or personal relationships that could have appeared to influence the work reported in this paper.

Acknowledgments

We have no grant and we also would like to thanks for Science Academy of Uzbekistan for their great contributions.

Declaration of Generative AI in Scientific Writing

The authors acknowledge the use of generative AI tools for language editing and grammar correction. No content generation or data interpretation was performed by AI. The authors take full responsibility for the content and conclusions of this work.

CRediT Author Statement

Bakiyeva Muazzam Sharifjanovna, **Gusakova Svetlana Valeryevna**: Conceptualization, Supervision, Project Administration, Writing - Review & Editing. **Sherzod Niyatqobulovich Zhurakulov**, **Xayitbayev Azamat Madaminovich**, **Xolmirzyeva Nazira Azimjon qizi**: Investigation, Methodology, Data Curation, Formal Analysis, Writing - Original Draft, Methodology, Laboratory Experiments, Data Collection. **Rustamova Shohista Omonjonovna**: Validation, Resources. **Dadamirzayeva Kamola Abduhalimovna**, **Xafizova Klaraxon Abdumannabovna**: Experimental Design, Investigation, Data Interpretation, Visualization. **Malanova Sadbar Abdukarimovna**: Software, Data Analysis, Figures Preparation. **Sharipova Nazifama Nasimovna**, Xodjayeva Naimaxon Umirzaqovna: Literature Review, Reference Management, Writing - Review & Editing. Yunusova Rayhona Melsbek qizi: Supervision, Funding Acquisition, Final Approval of the Manuscript.

Reference

[1] MSh Bakieva, SR Rustamova, TO Rakhmonov, NN Sharipova and KS Mukhitdinova. Hypotensive effect of the alkaloid benzoylheteratisine on the functional activity of rat aortic smooth muscle cells. *Academic Research Journal* 2022; **1(2)**, 24-30.

[2] J Park, S Shin, Y Kim, Y Bu, HY Choi and K Lee. Vasorelaxant and antihypertensive effects of the Cibotii Rhizoma hydroethanolic extract via the PI3K/AKT/eNOS pathway. *Phytomedicine* 2025; **148**, 157437.

[3] KKY Isla, MM Tanae, MTR de Lima-Landman, PM de Magalhães, AJ Lapa and C Souccar. Vasorelaxant effects of ellagitannins isolated from *Cuphea carthagenensis*. *Planta Medica* 2024; **90(4)**, 276-285.

[4] C Chen, C Guo, J Gao, K Shi, J Cheng, J Zhang, S Chen, Y Liu and A Liu. Vasorelaxant and antihypertensive effects of Tianshu Capsule on rats: An *in vitro* and *in vivo* approach. *Biomedicine & Pharmacotherapy* 2019; **111**, 188-197.

[5] J Jung, S Shin, J Park, K Lee and HY Choi. Hypotensive and vasorelaxant effects of Sanguisorbae Radix ethanol extract in spontaneously hypertensive and Sprague Dawley rats. *Nutrients* 2023; **15(21)**, 4510.

[6] P Wicha, A Onsa-Ard, W Chaichompoo, A Suksamrarn and C Tocharus. Vasorelaxant and antihypertensive effects of neferine in rats: An *in vitro* and *in vivo* study. *Planta Medica* 2020; **86(7)**, 496-504.

[7] N Shobako, A Ishikado, Y Ogawa, Y Sono, T Kusakari, M Suwa, M Matsumoto and K Ohinata. Vasorelaxant and antihypertensive effects that are dependent on the endothelial NO system exhibited by rice bran-derived tripeptide. *Journal of Agricultural and Food Chemistry* 2019; **67(5)**, 1437-1442.

[8] S Amtaghri, A Amssayef, M Slaoui and M Eddouks. Antihypertensive and vasorelaxant effects of *Hibiscus rosa-sinensis* through angiotensin-converting enzyme-2 (ACE-2), and Ca^{2+} channels pathways. *Cardiovascular & Hematological Disorders-Drug Targets* 2022; **22(1)**, 27-37.

[9] M Ajebli and M Eddouks. Vasorelaxant and antihypertensive effects of *Mentha pulegium* L. in rats: An *in vitro* and *in vivo* approach. *Endocrine, Metabolic & Immune Disorders-Drug Targets* 2021; **21(7)**, 1289-1299.

[10] NE Vega-Vela, D Osorio, M Avila-Rodriguez, J Gonzalez, LM García-Segura, V Echeverria and GE Barreto. L-type calcium channels modulation by estradiol. *Molecular Neurobiology* 2017; **54(7)**, 4996-5007.

[11] A Provence, KL Hristov, SP Parajuli and GV Petkov. Regulation of guinea pig detrusor smooth muscle excitability by 17β-estradiol: The role of the large conductance voltage- and Ca^{2+}-activated K^+ channels. *PLoS One* 2015; **10(11)**, e0141950.

[12] NJ Ortner and J Striessnig. L-type calcium channels as drug targets in CNS disorders. *Channels* 2016; **10(1)**, 7-13.

[13] D Lipscombe, TD Helton and W Xu. L-type calcium channels: The low down. *Journal of Neurophysiology* 2004; **92(5)**, 2633-2641.

[14] SJ Moore and GG Murphy. The role of L-type calcium channels in neuronal excitability and aging. *Neurobiology of Learning and Memory* 2020; **173**, 107230.

[15] MR Baker, AS Lee and AM Rajadhyaksha. L-type calcium channels and neuropsychiatric diseases: Insights into genetic risk variant-associated genomic regulation and impact on brain development. *Channels* 2023; **17(1)**, 2176984.

[16] B Robinson, Q Gu and J Kanungo. Antidepressant actions of ketamine: Potential role of L-type calcium channels. *Chemical Research in Toxicology* 2021; **34(5)**, 1198-1207.

[17] J Striessnig, NJ Ortner and A Pinggera. Pharmacology of L-type calcium channels: Novel drugs for old targets? *Current Molecular Pharmacology* 2015; **8(2)**, 110-122.

[18] AM Rajadhyaksha and BE Kosofsky. Psychostimulants, L-type calcium channels, kinases, and phosphatases. *The Neuroscientist* 2005; **11(5)**, 494-502.

[19] TP Giordano, TF Tropea, SS Satpute, MJ Sinnegger-Brauns, J Striessnig, BE Kosofsky and AM Rajadhyaksha. Molecular switch from L-type Cav 1.3 to Cav 1.2 Ca^{2+} channel signaling underlies long-term psychostimulant-induced

behavioral and molecular plasticity. *The Journal of Neuroscience* 2010; **30(50)**, 17051-17062.

[20] A Martínez-Rivera, J Hao, R Rice, CE Inturrisi and AM Rajadhyaksha. Cav1.3 L-type Ca^{2+} channel-activated CaMKII/ERK2 pathway in the ventral tegmental area is required for cocaine conditioned place preference. *Neuropharmacology* 2023; **224**, 109368.

[21] EJ Nunes and NA Addy. L-type calcium channel regulation of dopamine activity in the ventral tegmental area to nucleus accumbens pathway: Implications for substance use, mood disorders and co-morbidities. *Neuropharmacology* 2023; **224**, 109336.

[22] NA Addy, EJ Nunes, SM Hughley, KM Small, SJ Baracz, JL Haight and AM Rajadhyaksha. The L-type calcium channel blocker, isradipine, attenuates cue-induced cocaine-seeking by enhancing dopaminergic activity in the ventral tegmental area to nucleus accumbens pathway. *Neuropsychopharmacology* 2018; **43(12)**, 2361-2372.

[23] A Ghigo, A Perino, H Mehel, A Zahradníková Jr, F Morello, J Leroy, VO Nikolaev, F Damilano, J Cimino, E De Luca, W Richter, R Westenbroek, WA Catterall, J Zhang, C Yan, M Conti, AM Gomez, G Vandecasteele, E Hirsch and R Fischmeister. Phosphoinositide 3-kinase γ protects against catecholamine-induced ventricular arrhythmia through protein kinase A-mediated regulation of distinct phosphodiesterases. *Circulation* 2012; **126(17)**, 2073-2083.

[24] L Pinzi and G Rastelli. Molecular docking: Shifting paradigms in drug discovery. *International Journal of Molecular Sciences* 2019; **20(18)**, 4331.

[25] LG Ferreira, RN Dos Santos, G Oliva and AD Andricopulo. Molecular docking and structure-based drug design strategies. *Molecules* 2015; **20(7)**, 13384-13421.

[26] RN Dos Santos, LG Ferreira and AD Andricopulo. Practices in molecular docking and structure-based virtual screening. *Methods in Molecular Biology* 2018; **1762**, 31-50.

[27] JW Liang, S Wang, MY Wang, SL Li, WQ Li and FH Meng. Identification of novel PI3Kδ selective inhibitors by SVM-based multistage virtual screening and molecular dynamics simulations. *International Journal of Molecular Sciences* 2019; **20(23)**, 6000.

[28] A Bisht, D Tewari, S Kumar and S Chandra. Network pharmacology, molecular docking, and molecular dynamics simulation to elucidate the mechanism of anti-aging action of *Tinospora cordifolia*. *Molecular Diversity* 2024; **28(3)**, 1743-1763.

[29] K Crampon, A Giorkallos, M Deldossi, S Baud and LA Steffenel. Machine-learning methods for ligand-protein molecular docking. *Drug Discovery Today* 2022; **27(1)**, 151-164.

[30] M Batool, B Ahmad and S Choi. A structure-based drug discovery paradigm. *International Journal of Molecular Sciences* 2019; **20(11)**, 2783.

[31] X Yang, Y Wang, R Byrne, G Schneider and S Yang. Concepts of artificial intelligence for computer-assisted drug discovery. *Chemical Reviews* 2019; **119(18)**, 10520-10594.

[32] S Sharma and D Sharma. Intelligently applying artificial intelligence in chemoinformatics. *Current Topics in Medicinal Chemistry* 2018; **18(20)**, 1804-1826.

[33] J Jiménez-Luna, F Grisoni, N Weskamp and G Schneider. Artificial intelligence in drug discovery: Recent advances and future perspectives. *Expert Opinion on Drug Discovery* 2021; **16(9)**, 949-959.

[34] ZX Chen, YS Qin, BH Shi, BY Gao, RC Tao and XZ Yong. Effects of curcumin on radiation/chemotherapy-induced oral mucositis: Combined meta-analysis, network pharmacology, molecular docking, and molecular dynamics simulation. *Current Issues in Molecular Biology* 2024; **46(9)**, 10545-10569.

[35] Katifelis, H.; Grammatikaki, S.; Zakopoulou, R.; Bamias, A.; Karamouzis, M.V.; Stravodimos, K.; Gazouli, M. Up-regulation of

[36] Cuproptosis-related lncRNAS in Patients Receiving Immunotherapy for Metastatic Clear Cell Renal Cell Carcinoma Indicates

[37] Progressive Disease. In Vivo 2025, 39, 146–151AJPO de Almeida, TP Ribeiro and IA de Medeiros. Aging: Molecular pathways and implications on the cardiovascular system.

Oxidative Medicine and Cellular Longevity 2017; **2017**, e7941563.

[38] B Wu, G Ge, J Xu, Y Xing, K Hu, J Ren and J Yang. 12-ethoxy-Marchantin A, a new macrocyclic bis-bibenzyl from *Marchantia polymorpha* L., exerts anti-aging activity through activating MAPKs-dependent NrF3/HO-1 signaling pathways. *Biogerontology* 2025; **26(5)**, 189.

[39] M Noda, Y Takuwa, T Katoh and K Kurokawa. Mechanical force regulation of vascular parathyroid hormone-related peptide expression. *Kidney International Supplement* 1996; **55**, S154-S155.

[40] Y Nishizawa, H Koyama, A Shioi, M Hosoi, S Jono, M Hino and H Morii. Parathyroid hormone-related peptide and models of vascular disease: Its expression and action in vascular smooth muscle cells. *Mineral and Electrolyte Metabolism* 1995; **21(1-3)**, 152-156.

[41] KP Malabanan, P Kanellakis, A Bobik and LM Khachigian. Activation transcription factor-4 induced by fibroblast growth factor-2 regulates vascular endothelial growth factor-A transcription in vascular smooth muscle cells and mediates intimal thickening in rat arteries following balloon injury. *Circulation Research* 2008; **103(4)**, 378-387.

[42] K Friend, HA Brooks, NE Propson, JA Thomson and J Kimble. Embryonic stem cell growth factors regulate eIF3α phosphorylation. *PLoS One* 2015; **10(9)**, e0139076.

[43] GK Owens, MS Kumar and BR Wamhoff. Molecular regulation of vascular smooth muscle cell differentiation in development and disease. *Physiological Reviews* 2004; **84(3)**, 767-801.

[44] M Miyoshi, T Shimosato and T Takaya. Myogenic anti-nucleolin aptamer iSN04 inhibits proliferation and promotes differentiation of vascular smooth muscle cells. *Biomolecules* 2024; **14(6)**, 709.

[45] GA Roth, GA Mensah, CO Johnson, G Addolorato, E Ammirati, LM Baddour, NC Barengo, AZ Beaton, EJ Benjamin and CP Benziger. Global burden of cardiovascular diseases and risk factors, 1990-2019: Update from the GBD 2019 study. *Journal of the American College of Cardiology* 2020; **76**, 2982-3021.

[46] E Mahdinia, N Shokri, AT Taheri, S Asgharzadeh, M Elahimanesh and M Najafi. Cellular crosstalk in atherosclerotic plaque microenvironment. *Cell Communication and Signaling* 2023; **21**, 125.